NASA TECHNICAL MEMORANDUM

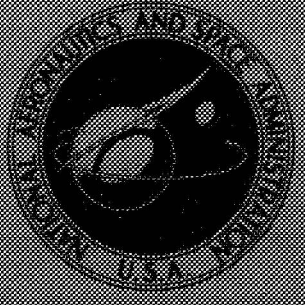

N71-17554

NASA TM X-2173

NASA TM X-2173

CASE FILE COPY

PERFORMANCE OF AN AUXILIARY INLET EJECTOR NOZZLE WITH FLOATING INLET DOORS AND FLOATING SINGLE-HINGE TRAILING-EDGE FLAPS

by Albert L. Johns

Lewis Research Center

Cleveland, Ohio 44135

NATIONAL AERONAUTICS AND SPACE ADMINISTRATION • WASHINGTON, D. C. • FEBRUARY 1971

CONTENTS

PERFORMANCE OF AN AUXILIARY INLET EJECTOR NOZZLE WITH FLOATING INLET DOORS AND FLOATING SINGLE-HINGE TRAILING-EDGE FLAPS

by Albert L. Johns
Lewis Research Center

SUMMARY

An aerodynamically positioned auxiliary inlet ejector nozzle which is applicable to a turbojet engine in a supersonic-cruise aircraft was tested in the 8- by 6-Foot Supersonic Wind Tunnel to determine the performance characteristics over a range of free-stream Mach numbers from 0 to 1.0. Room-temperature air was used as the primary and secondary fluid. Two different primary throat areas were used: one to simulate both dry acceleration and subsonic cruise, and a larger one to simulate reheat operation.

The auxiliary inlet doors included both single- and double-hinge types which were free-floating either with or without synchronization. The secondary shroud had free-floating, single-hinge trailing-edge flaps that provided an internal area ratio variation from 2.10 to 3.74 for the small primary and from 1.53 to 2.68 for the large primary. The corrected secondary weight flow was generally held constant at a nominal 4 percent of the primary flow. At some flight conditions, the secondary flow was varied to determine its effect on performance. In general, at subsonic-cruise conditions the inlet doors and trailing-edge flaps did not float to the optimum thrust condition. For example, at Mach 0.90 and a nozzle pressure ratio of 3.2, the gross thrust coefficient of the floating configuration was about 0.87. This configuration was 4 percent lower than a similar nozzle optimized with fixed components. The trailing-edge flaps floated off the inner stops and increased the internal expansion. At the same condition, the inlet doors floated about half closed. The overall effect was a nozzle that was overexpanded and provided low subsonic-cruise efficiency. In addition, the single-hinge trailing-edge flaps were unstable at many of the assumed trajectory flight conditions. At subsonic cruise the instability occurred at high frequency (much greater than 24 Hz) with small amplitude oscillation from 1.2 to 1.5 percent of the model diameter and frequently caused model damage. At the higher pressure ratios for dry acceleration the nature of the instability was low-frequency (2 to 5 Hz), large-amplitude oscillation from 4 to 12 percent of the model diameter and nondestructive. An instability occurred at takeoff with reheat, but was eliminated by positioning the inner stop to increase the minimum exit area. This instability was high-frequency, small-amplitude oscillation and resulted in model failure.

Double-hinge inlet doors provided a slightly higher thrust efficiency at subsonic cruise than a single-hinge door. However, there was little difference in performance whether the doors were synchronized or not.

INTRODUCTION

As part of a current program in airbreathing propulsion, the Lewis Research Center is evaluating various exhaust nozzle concepts which are appropriate for supersonic-cruise aircraft. Ideally, these nozzles should operate efficiently over a wide range of flight conditions and engine power settings. Requirements such as these usually necessitate extensive variation in nozzle geometry, including both the primary nozzle throat and shroud exit areas. The performance of a variable flap ejector and a low-angle plug nozzle designed for a supersonic-cruise aircraft is reported in references 1 and 2. Another nozzle type of interest is the auxiliary inlet ejector (refs. 3 and 4). At low power settings the auxiliary inlets open to admit tertiary air to prevent overexpansion of the primary jet. Hence, there is a reduced requirement for exit-area variation and a corresponding reduction in boattail angle and projected area.

This report documents the aerodynamic performance of an auxiliary inlet ejector nozzle with both the inlet doors and single-hinge trailing-edge flaps aerodynamically positioned. The primary nozzle used in this test simulated the General Electric J85-GE-13 afterburning turbojet engine currently being used in an F-106B flight test program at Lewis.

The model has a diameter of 8.50 inches (21.59 cm) and was tested in the Lewis 8- by 6-Foot Supersonic Wind Tunnel at free-stream Mach numbers from 0 to 1.0 and over a range of nozzle pressure ratios from 2.0 to 6.0. Secondary weight flow was varied from 0 to approximately 15 percent of the primary nozzle weight flow at takeoff and at subsonic-cruise Mach numbers. Dry air at room temperature was used for both the primary and secondary weight flows. The results from this test are compared with those of a similar nozzle which was optimized using fixed inlet doors and flaps.

APPARATUS AND PROCEDURE

Installation in Wind Tunnel

A schematic view of the model support system in the 8- by 6-Foot Supersonic Wind Tunnel, showing the internal geometry and thrust-measuring system, is presented in figure 1. Symbols are defined in the appendix. The grounded portion of the model was supported from the tunnel ceiling by a vertical strut. The floating portion was attached to the primary and secondary air bottles which were cantilevered by flow tubes from external supply manifolds. The primary air bottle was supported by front and rear bearings. The secondary air passed through an annulus around the primary nozzle. The axial force of the nozzle, which included secondary and tertiary flow effects, was trans-

mitted to the load cell located in the nose of the model. Since the floating portion of the model included the afterbody and boattail, the measured force was that resulting from the interaction of the internal and external flows. General external flow characteristics of this 8.5-inch (21.6-cm) jet-exit model are described in reference 5.

Force Measurements

Thrust-minus-drag measurements were obtained from a load-cell readout of the axial forces acting on the floating portion of the model. Internal tare forces determined by internal areas, and measured tare pressures located as shown in figure 1, were accounted for in the thrust calculation.

A static calibration of the thrust-measuring system was obtained by applying known forces to the nozzle and measuring the output of the load cell. A water-cooled jacket surrounded the load cell and maintained a constant temperature of 90° F (305 K) to eliminate errors in the calibration caused by variations in temperature from aerodynamic heating.

The only external friction drag charged to the nozzle was that downstream of model station 122.84 inches (312 cm), figure 1. The force acting on the portion of the nozzle between model station 93.65 inches (238 cm) and 122.84 inches (312 cm) was measured on the load cell; however, it was not considered to be part of the nozzle drag. Its magnitude was estimated by using the semi-empirical, flat plate, mean skin friction coefficient given in figure 7 of reference 6 as a function of free-stream Mach number and Reynolds number. Previous measurements of the boundary-layer characteristics at the aft end of the jet-exit model in the 8- by 6-Foot Supersonic Wind Tunnel (ref. 7) indicated that the profile and thickness were essentially the same as that computed for a flat plate of equal length. The strut wake appeared to affect only a localized region near the top of the model and resulted in a slightly lower local free-stream velocity than measured on the side and bottom of the model. Therefore, the results of reference 6 were used without correction for three-dimensional flow effects or strut interference effects.

The secondary flow rate was measured by means of a standard ASME flowmetering orifice located in the external supply line. The primary flow was calculated from a previously measured flow coefficient at the throat station (ref. 4). Two choke plates and a straightening screen were utilized to provide a good profile to the internal flow approaching the nozzle inlet. The ideal jet thrust of the primary flow was calculated from its measured mass-flow rate expanded from its measured total pressure (P_7) to free-stream static pressure p_0. Nozzle gross-thrust coefficient is defined as the ratio of the measured thrust-minus-drag to the ideal thrust of the primary:

$$\text{Nozzle gross-thrust coefficient} = \frac{F - D}{F_{i,p}}$$

Nozzle Configurations

Various configurations of the nozzle installed in the wind tunnel are shown in figure 2. Basic parameters of the auxiliary inlet ejector nozzle are shown in figure 3. A General Electric J85-GE-13 primary nozzle was simulated for this test, as shown. Two different primary throat areas were used. The small throat area was used to simulate dry acceleration and subsonic cruise. The larger area simulated reheat operation. Additional details of the simulated J85 primary nozzles are shown in figure 4. As mentioned earlier, primary weight flow was calculated using the measured values of the discharge coefficient listed for the two primary areas. The variable primary nozzle actuating mechanism blockage was simulated by a ring containing 12 slots. Secondary air was diverted through these slots by means of a deflector to simulate primary flap cooling air.

Details of the auxiliary inlets are shown in figure 5. Two types of auxiliary inlets were tested: double-hinge doors as shown in figure 5(a) and single-hinge doors as shown in figure 5(b). Each auxiliary inlet configuration contained 16 doors and 16 equally spaced ribs. The single-hinge doors were tested free-floating both synchronized and unsynchronized. The double-hinge doors were also tested free-floating synchronized and unsynchronized with the angle of the second inlet ramp restrained to be twice the angle of the initial ramp. One additional double-hinge configuration was tested in which unsynchronized doors were used with no restraint on the relation between the first and second ramp angles.

The aerodynamically positioned, trailing-flap section consisted of 16 overlapping single-hinge flaps (fig. 6). The projected boattail area varied from 44 percent (fully closed position) to zero percent (fully open) of the simulated nacelle area A_{max}. The inner stops were positioned such that the trailing-flap exit area (station 9) was always greater than the secondary-shroud minimum area. The variation of internal area ratio A_9/A_8 is given in figure 7 as a function of the boattail angle β for both primary nozzles.

Nozzle Instrumentation

The instrumentation at station 7 (nozzle inlet station) and the static-pressure orifices on the primary nozzle are shown in figures 8(a) and (b). The secondary passage base (upstream of the primary nozzle boattail) static orifices were located circumferentially at 10^o, 100^o, 190^o, and 280^o. A row of four static-pressure orifices were located

on the primary nozzle boattail at 90°. In addition, a single orifice was located on the primary nozzle base, also at 90°. One static-pressure orifice was also located at 0° on the outer surface of the ring simulating the actuation mechanism blockage. The primary, secondary, and tertiary total pressures were obtained from total-pressure probes located as shown in figures 8(b) and (c). A row of static-pressure orifices were located at 90° on the flap internal surface and at 180° along the external boattail (fig. 8(c)). An external row of static-pressure orifices was located on the door at 180° (fig. 8(d)).

Primary-total-pressure profiles of the internal flow entering the primary nozzle are shown in figure 9. As expected, the profiles were relatively flat with both primary nozzles. The nozzle inlet total pressure P_7 was obtained by integrating the pressure across an area-weighted rake located in the primary flow passage at station 7. The flow was assumed to be circumferentially uniform.

Procedure

Nozzle performance was obtained over a range of free-stream Mach numbers and nozzle pressure ratios. For several of the figures, results are presented with the assumption of a nozzle pressure ratio schedule appropriate for a turbojet engine cycle (fig. 10). At a given Mach number the nozzle pressure ratio was varied around the value shown by changing the nozzle inlet total pressure. Secondary weight flow was varied from 0 to 15 percent of the primary flow at takeoff and over a range of subsonic-cruise Mach numbers. The results herein are compared with those of a similar nozzle which was optimized using fixed inlet doors and flaps. The position of the free-floating doors and flaps was measured from motion-picture films taken during the test. The instability conditions were observed during the test and from the films taken.

RESULTS AND DISCUSSION

The performance of the nozzles over the trajectory specified in figure 10 is presented initially in figures 11 to 16 for a nominal secondary-weight-flow ratio of 4 percent. Some of the more pertinent instability points are summarized in figure 17. Then the effect on performance of variations in nozzle pressure ratio and secondary flow is presented in figures 18 to 21 for all the configurations tested.

Performance Comparisons for Assumed Flight Trajectory

At subsonic cruise the performance obtained with aerodynamically positioned doors and flaps was generally less than that obtained for a similar nozzle with fixed components (fig. 11(a) and (b)). For example, at Mach 0.90 with the single-hinge doors (fig. 11(a)), the gross thrust coefficients were approximately 0.84 and 0.89 for the nozzle with floating and fixed components, respectively. The gross thrust coefficients for the double-hinge door configuration at Mach 0.90 were approximately 0.87 for the nozzle with floating components and about 0.91 for the nozzle with fixed components (fig. 11(b)). Peak performance at these flight conditions with fixed hardware was obtained with the trailing-edge flaps on the inner stops (minimum A_9) and the inlet doors nearly full open, as shown in figures 11(a) and (b) from the results presented in reference 4. The results presented herein indicate that the inlet doors and trailing-edge flaps did not float to the maximum thrust position. With external flow, the trailing-edge flaps generally floated off the inner stops at low pressure ratios and increased the internal expansion. At the same time, the inlet doors were partially closed and reduced the flow of tertiary air that is required to prevent the overexpansion of the primary jet. Although the primary flow is separated from the shroud at this condition, the overall effect was a nozzle that was overexpanded with a corresponding loss in gross thrust coefficient. There was little difference in performance whether the doors were synchronized or not. The secondary total pressure was slightly less than free-stream static pressure. In contrast, the secondary total pressure obtained with the hardware fixed for maximum thrust was always greater than free-stream static pressure, indicating higher pressures in the primary nozzle base region.

The effect of external flow on nozzle pressure distribution is shown in figure 12, where static results are compared to those at Mach 0.90 for a nozzle pressure ratio of about 3.20. The overall effect was a 14-percent loss in gross thrust coefficient when compared with static performance at approximately the same pressure ratio. With external flow, the trailing-edge flaps float off the inner stops, thereby increasing the internal area ratio. The inlet doors floated partially closed. The resulting overexpansion of the nozzle is evident in the static-pressure variations shown in figure 12. The pressures are particularly low on the internal rearward-facing surface of the secondary shroud ahead of the trailing-edge flap. The overall performance is further degraded by the external boattail and inlet door drag.

The performance of the synchronized and the unsynchronized single-hinge inlet door configurations is shown in figure 13 for the assumed trajectory. There was little difference in performance whether the inlet doors were synchronized or not. The trailing-edge flaps were on the inner stops at takeoff and during dry acceleration. However, at subsonic-cruise conditions with the pressure ratio reduced, the flaps float open, as mentioned previously. This configuration would not pump 4-percent cooling flow at

takeoff conditions. However, the pumping characteristics (in figs. 20 and 21) indicate that it can pump some smaller amount of cooling flow at takeoff, of the order of 2 to 3 percent of the primary flow.

The conclusions obtained for the single-hinge door configurations also generally apply to the three double-hinge door configurations that were tested (fig. 14). Synchronization had little effect on performance. The trailing-edge flaps again floated off the inner stops when the pressure ratio was reduced for subsonic cruise.

As shown in figure 15 for subsonic-cruise conditions, the double-hinge inlet door configuration provided a slightly higher thrust efficiency than the single-hinge inlet door.

Reheat acceleration data presented in figure 16 were only obtained for one double-hinge inlet door configuration. Floating performance was slightly better than that measured with the fixed hardware (ref. 4). In the previous test the flaps were fixed on the inner stops (ref. 4) and it was observed that high pressures existed internally on the converging trailing-edge flaps, with a resultant loss in internal performance. These higher pressures caused the flaps of the current model to float off the inner stops and reduced both the convergence of the flaps and the internal losses. As predicted with the fixed hardware, the inlet doors were closed at Mach numbers from 0.60 to 0.95. The pumping characteristics obtained with the floating hardware were quite similar to those obtained with the fixed components.

Nozzle Stability

In addition to the low performance obtained at subsonic cruise with the floating hardware, the single-hinge trailing-edge flaps were unstable at many of the assumed trajectory conditions. All measured instability points are identified on the general performance figures (figs. 18 to 21) with tailed symbols. The instabilities occurring at a nominal 4-percent corrected-secondary-weight-flow ratio are summarized in figure 17 and compared with the trajectory conditions. These instabilities were observed and photographed during the test program. However, the cycles per second of the high-frequency instabilities were well beyond the range of the 24-frame-per-second camera used during the test. In general, the instabilities can be classified into two groups. The instability observed at subsonic-cruise conditions was characterized by high-frequency (much higher than 24 Hz), small-amplitude oscillations from 1.2 to 1.5 percent of the model diameter that generally resulted in damage to the model. The flaps were off the inner stops when the instabilities were encountered. At this condition the nozzle was generally operating at a low pressure ratio ($P_7/p_0 < 4.0$), while the internal expansion was large ($A_9/A_8 \geq 2.4$). As shown in the pressure distribution in figure 12, the flow overexpands in the initial part of the secondary shroud, separates from the walls, and shocks back to

ambient pressure. This condition when encountered with floating flaps can cause an instability problem. This type of aeroelastic instability has been observed before and was described in detail in reference 8, as "high-area-ratio separation buffeting."

A second type of instability observed in this test was also discussed rather thoroughly in reference 8 as "low-area-ratio vibration." This instability occurred at the pressure ratios for dry acceleration and was characterized by low-frequency (2 to 5 Hz), large amplitude oscillations varying from 4 to 12 percent of the model diameter that generally were nondestructive to the model. At pressure ratios slightly below this flight condition, the flaps were on the inner stops and were stable. In this condition the maximum secondary shroud area occurs between the throat and exit station, resulting in a converging-diverging nozzle followed by convergence in the flap section. As discussed in reference 8, the instability occurs at higher pressure ratios when the recompression of the internal attached flow makes a sudden transition from a normal shock to an oblique shock as pressure ratio is increased slightly. This transition, which was observed in the present test to be very abrupt, caused the nozzle flaps to open suddenly (off the inner stops) and then oscillate at a low frequency (2 to 5 Hz). Static-pressure measurements along the flap section with fixed hardware (ref. 4) clearly indicated the large change in flap pressures that can occur during this transition with a slight change in nozzle pressure ratio.

One other unstable point was observed at takeoff with the large reheat primary. This instability was high-frequency (greater than 24 Hz), small-amplitude (oscillation varying from 1.2 to 1.5 percent of the model diameter) and resulted in a failure of the trailing-edge flaps. This instability was eliminated by increasing the minimum area-ratio of the nozzle from 1.47 to 1.53.

All the auxiliary inlet door configurations were stable with the exception of the double-hinge unsynchronized doors with no restraint on the relation of first and second ramp angles. These inlet doors oscillated rather frequently at all Mach numbers above static conditions. However, the oscillation did not result in damage to the model. The unsynchronized door configurations had some unsymmetrical door movement with external flow.

Effect of Nozzle Pressure Ratio on Performance Characteristics

The effect of nozzle pressure ratio on nozzle gross thrust coefficient, pumping characteristics, and boattail angle is presented in figures 18 and 19 for the single- and double hinge inlet door configurations, respectively. Data are presented over the range of Mach numbers tested for both the small and large primary with a nominal corrected-secondary-weight-flow ratio of 0.04. In general, with the small primary, external flow caused a

substantial loss in gross thrust coefficient, especially at the lower values of nozzle pressure ratio. At these same conditions, the floating flaps were generally off the inner stops, the inlet doors were partly closed, and the nozzle was overexpanded. The floating flaps were only on the inner stops at static conditions and at nozzle pressure ratios greater than 4.5 or 5.0. Two tailed symbols at a given pressure ratio indicate the magnitude of the flap deflection during an unstable condition. The secondary total pressure was generally equal to free-stream static pressure at the lower pressure ratios and slightly higher at pressure ratios greater than 4.0. Pumping characteristics were generally independent of external flow effects.

External flow effects were generally small for the large primary nozzle (fig. 19(d)). Pumping characteristics again were not affected by external flow and the secondary total pressures were higher than free-stream static pressure. In most cases, the trailing-edge flaps were nearly closed but were starting to open at the higher values of nozzle pressure ratio. The inlet doors were also nearly or fully closed.

Effect of Corrected Secondary Weight Flow on Performance Characteristics

The effect of corrected-secondary-weight flow ratio on nozzle gross thrust coefficient, pumping characteristics, and boattail angle is presented in figures 20 and 21 for the single- and double-hinge inlet door configurations, respectively. Data are presented for several free-stream Mach numbers at a pressure ratio near the assumed trajectory value. For two configurations (figs. 20(a) and 21(a)), the ram drag of the secondary flow was subtracted from the measured thrust-minus-drag at Mach numbers of 0.85 and 0.90. These results indicate that the equivalent gross thrust coefficient $\left[(F - D) - m_s V_0\right]/F_{ip}$ was not improved with addition of secondary flow. In some cases the addition of secondary flow reduced the nozzle boattail angle but had little effect on inlet door position, except for the large primary at static conditions (fig. 21(d)). At this condition the addition of secondary flow pressurized the primary nozzle base region causing the inlet doors to move from a full open to an in-travel condition. It was also observed that secondary flow had no effect in reducing or eliminating trailing-edge-flap instabilities.

SUMMARY OF RESULTS

An experimental investigation was conducted to determine the performance characteristics of an aerodynamically positioned auxiliary inlet ejector nozzle which is applicable

to a supersonic-cruise aircraft. The nozzle performance was obtained over a range of free-stream Mach numbers from 0 to 1.0 and nozzle pressure ratios from 2 to 6. Two different-size primary throat areas were used: a small throat to simulate both subsonic cruise and dry acceleration, and a large throat to simulate reheat acceleration. The auxiliary inlet doors included both free-floating single- and double-hinge types that were either synchronized or unsynchronized when tested. The secondary shroud had free-floating, single-hinge trailing-edge flaps that provided an internal-area-ratio A_9/A_8 variation from 2.10 to 3.74 for the small primary and from 1.53 to 2.68 for the large primary. The corrected secondary weight flow was generally held constant at 4 percent of the primary flow. However, at some flight conditions the secondary flow was varied to determine its effect on performance. The following results were obtained for an assumed turbojet trajectory and a nominal corrected secondary flow of 4 percent of the primary flow:

1. The single-hinge, trailing-edge flaps were unstable at many of the assumed trajectory flight conditions. At subsonic cruise the characteristic of the instability was high-frequency (greater than 24 Hz), small-amplitude oscillation varying from 1.2 to 1.5 percent of the model diameter and several times resulting in model damage. At the higher nozzle pressure ratios for dry acceleration, the nature of the instability was low-frequency (2 to 5 Hz), large-amplitude oscillation varying from 4 to 12 percent of the model diameter and nondestructive. An instability occurred at takeoff with reheat, but was eliminated by positioning the inner stops to increase the minimum exit area. The instability was of high-frequency, small-amplitude oscillation and resulted in model failure.

2. In general, the inlet doors and trailing-edge flaps did not float to the maximum thrust condition. For example, with double-hinge doors at subsonic cruise, Mach 0.90, and a nozzle pressure ratio of 3.2, the gross thrust coefficient of the floating configuration was approximately 0.87. This value was about 4 percent lower than that determined for a similar nozzle with fixed inlet doors and flap.

3. External flow caused a substantial loss in nozzle gross thrust coefficient at the subsonic-cruise pressure ratio. For example, at Mach 0.90, and pressure ratio of 3.2, the trailing-edge flaps floated off the inner stops and increased the internal expansion. At the same condition the double-hinge inlet doors floated about half closed. The overall effect was a 14-percent loss in gross thrust coefficient compared with static performance at nearly the same pressure ratio.

4. There was little difference in performance whether the doors were unsynchronized or synchronized.

5. Double-hinge inlet doors provided a slightly higher gross thrust coefficient than the single-hinge inlet doors.

Lewis Research Center,
National Aeronautics and Space Administration,
Cleveland, Ohio, September 23, 1970,
720-03.

APPENDIX - SYMBOLS

A	area
C_d	nozzle flow coefficient
D	drag
d	diameter
d_e	outside diameter of primary nozzle base
F	thrust
$\frac{F - D}{F_{i,p}}$	nozzle gross thrust coefficient
$\frac{(F - D) - m_s v_0}{F_{i,p}}$	equivalent gross thrust coefficient (equates duel-flow nozzle to a single-flow nozzle)
L	axial distance from nozzle throat (station 8) to nozzle exit (station 9)
L_p	primary nozzle flap length
M	Mach number
m	mass-flow rate
P	total pressure
p	static pressure
R	radius of primary airflow passage at station 7
r	radial distance from center of primary airflow passage at station 7 to local orifice
S	axial distance from nozzle throat to minimum shroud diameter
T	total temperature
V	velocity
w	weight-flow rate
α	primary nozzle flap angle, deg
β	boattail angle, deg
δ	door position, deg
θ	circumferential position measured clockwise from top of model, deg

$\omega\sqrt{\tau}$	corrected-secondary-weight-flow ratio $(w_s/w_p)\sqrt{T_s/T_p}$

Subscripts:

i	ideal
l	local
max	nacelle
p	primary
r	radial distance from center of primary airflow passage at station 7 to local orifice
S	shroud
s	secondary
ter	tertiary
1	upstream door
2	downstream door

Stations:

0	free stream
7	nozzle inlet
8	nozzle throat
9	nozzle exit

REFERENCES

1. Steffen, Fred W.; and Jones, John R.: Performance of a Wind Tunnel Model of an Aerodynamically Positioned Variable Flap Ejector at Mach Numbers From 0 to 2.0. NASA TM X-1639, 1968.
2. Bresnahan, Donald L.: Experimental Investigation of a 10^{o} Conical Turbojet Plug Nozzle With Iris Primary and Translating Shroud at Mach Numbers From 0 to 2.0. NASA TM X-1709, 1968.
3. Shrewsbury, George D.; and Jones, John R.: Static Performance of an Auxiliary Inlet Ejector Nozzle for Supersonic-Cruise Aircraft. NASA TM X-1653, 1968.
4. Johns, Albert L.; and Steffen, Fred W.: Performance of an Auxiliary Inlet Ejector Nozzle With Fixed Doors and Single-Hinge Trailing-Edge Flap. NASA TM X-2027, 1970.
5. Blaha, Bernard J.; and Bresnahan, Donald L.: Wind Tunnel Installation Effects on Isolated Afterbodies at Mach Numbers From 0.56 to 1.50. NASA TM X-52581, 1969.
6. Smith, K. G.: Methods and Charts for Estimating Skin Friction Drag in Wind Tunnel Tests With Zero Heat Transfer. Rep. ARC-CP-824, Aeronautical Research Council, Great Britain, 1965.
7. Harrington, Douglas E.: Jet Effects on Boattail Pressure Drag of Isolated Ejector Nozzles at Mach Numbers From 0.60 to 1.47. NASA TM X-1785, 1969.
8. Alford, J. S.; and Taylor, R. P.: Aerodynamic Stability Considerations of High-Pressure Ratio, Variable-Geometry Jet Nozzles. J. Aircraft, vol. 2, no. 4, July-August 1965, pp. 308-311.

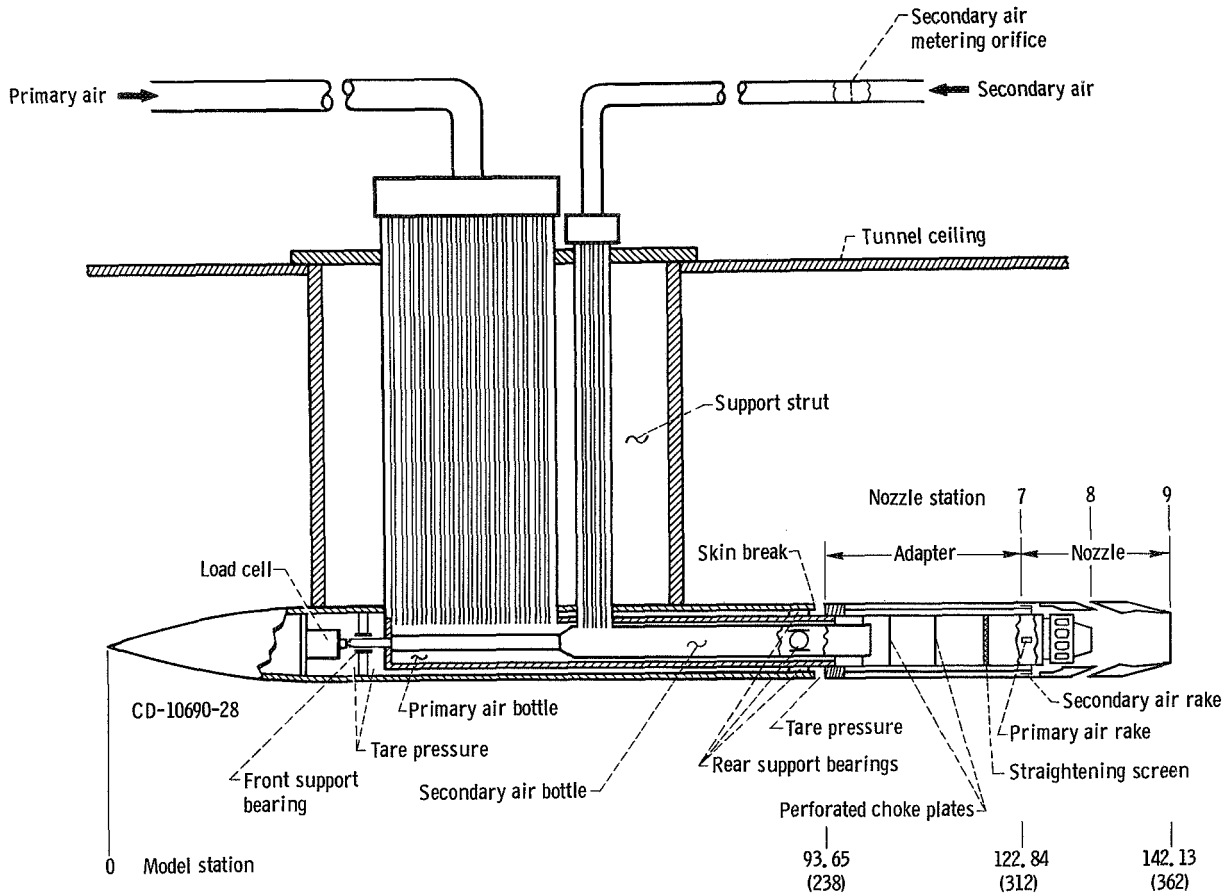

Figure 1. - Nozzle support model and thrust measuring system. (Dimensions are in inches (cm).)

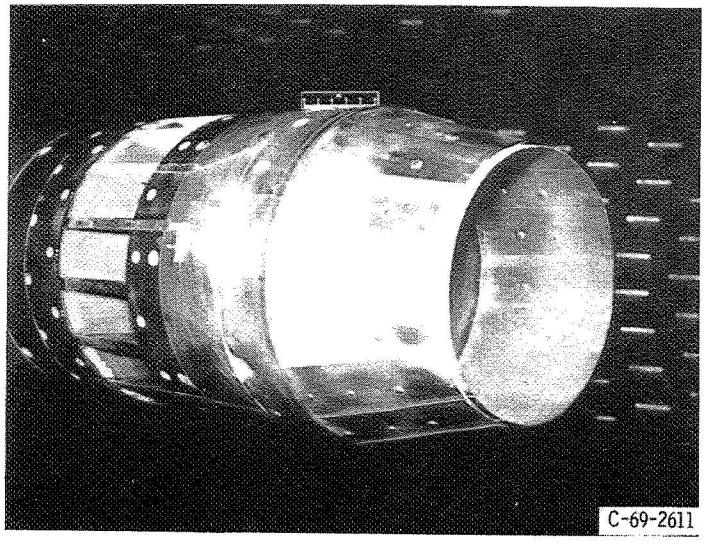

(a) Single-hinge doors with flaps closed.

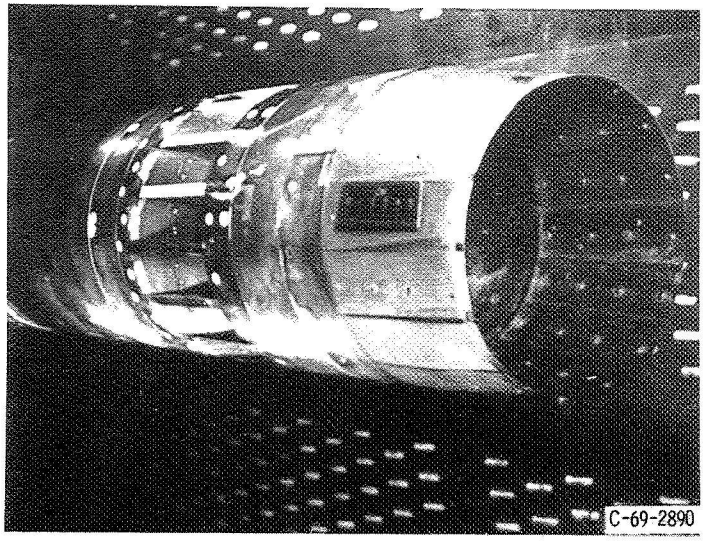

(b) Double-hinge doors with flaps open.

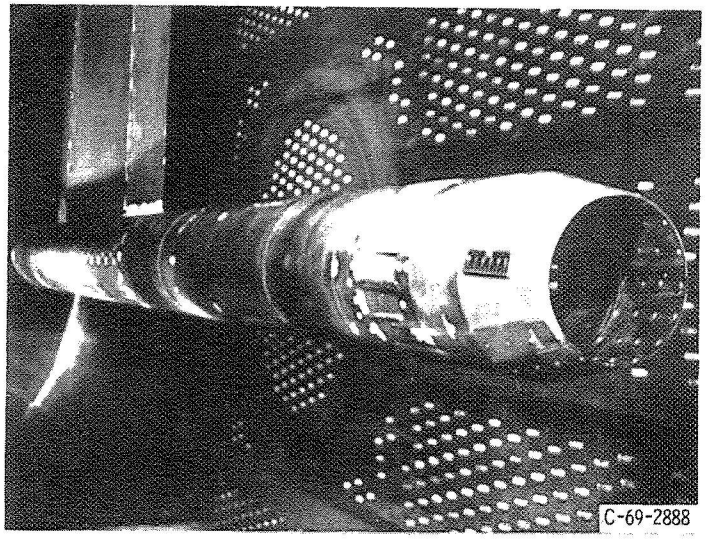

(c) Overall view of model installed in 8- by 6-Foot Supersonic Wind Tunnel.

Figure 2. - Aerodynamically positioned auxiliary inlet ejector nozzle.

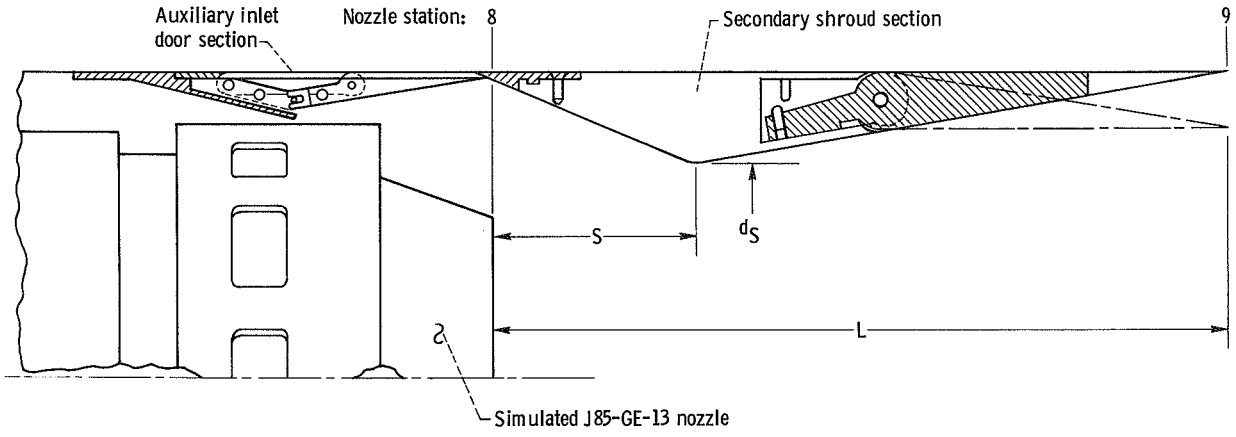

Primary nozzle configuration	Ratio of nozzle throat area to simulated nacelle area, A_8/A_{max}	Flight simulation	Internal area ratio, A_9/A_8		Spacing ratio, S/d_8	Diameter ratio, d_S/d_8	Flap length ratio, L/d_8
			Maximum	Minimum			
Small	0.267	Dry acceleration, subsonic cruise	3.74	2.10	0.756	1.408	2.35
Large	0.373	Reheat acceleration	2.68	1.53	0.720	1.190	2.06

Figure 3. - Basic parameters for auxiliary inlet ejector nozzle.

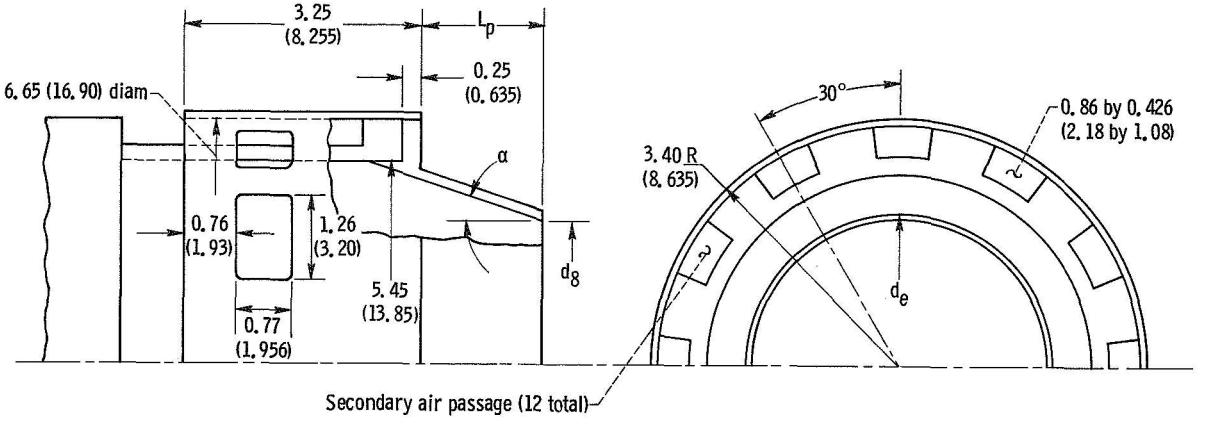

Primary nozzle diameter, d_8	Primary nozzle flap angle, α, deg	Primary nozzle flap length, L_p	Outside diameter of primary nozzle base, d_e	Nozzle flow coefficient, C_d
4.388 (11.146)	13.25	1.50 (3.810)	4.622 (11.74)	0.977
5.192 (13.188)	5.30	1.08 (2.743)	5.437 (13.81)	0.985

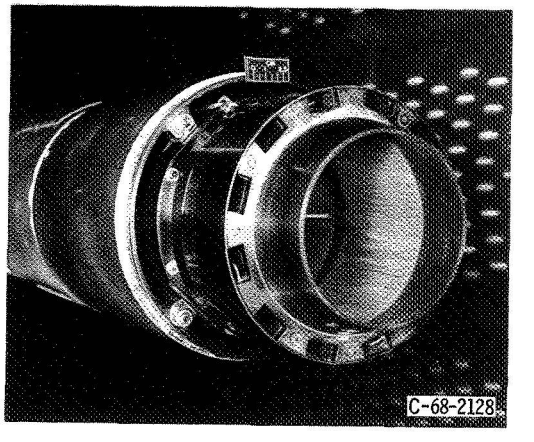

Figure 4. - Details of simulated J85-GE-13 primary nozzle. (Dimensions are in inches (cm).)

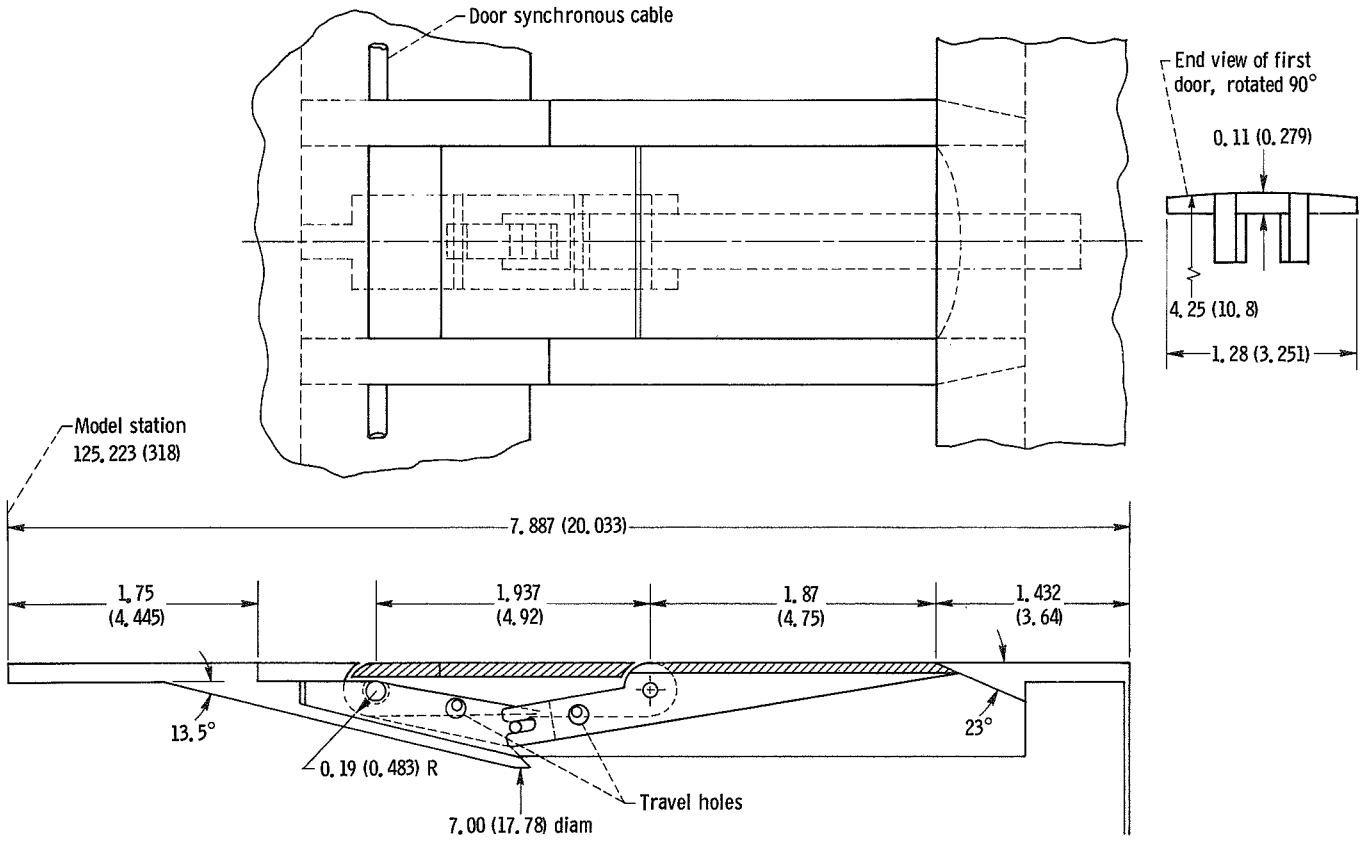

(a) Double-hinge door.

Figure 5. - Details of auxiliary inlets. (Dimensions are in inches (cm).)

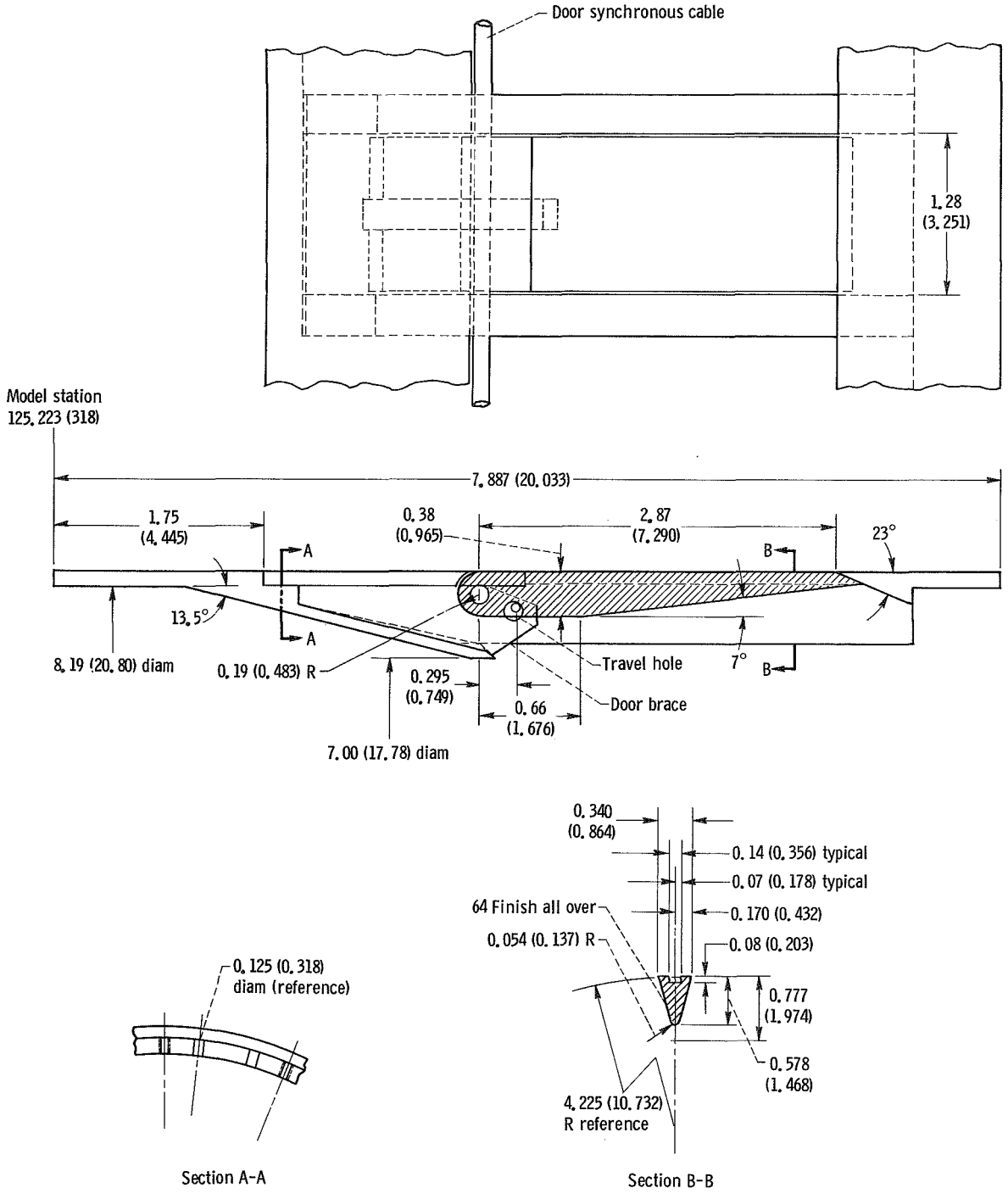

(b) Single-hinge door.

Figure 5. - Concluded.

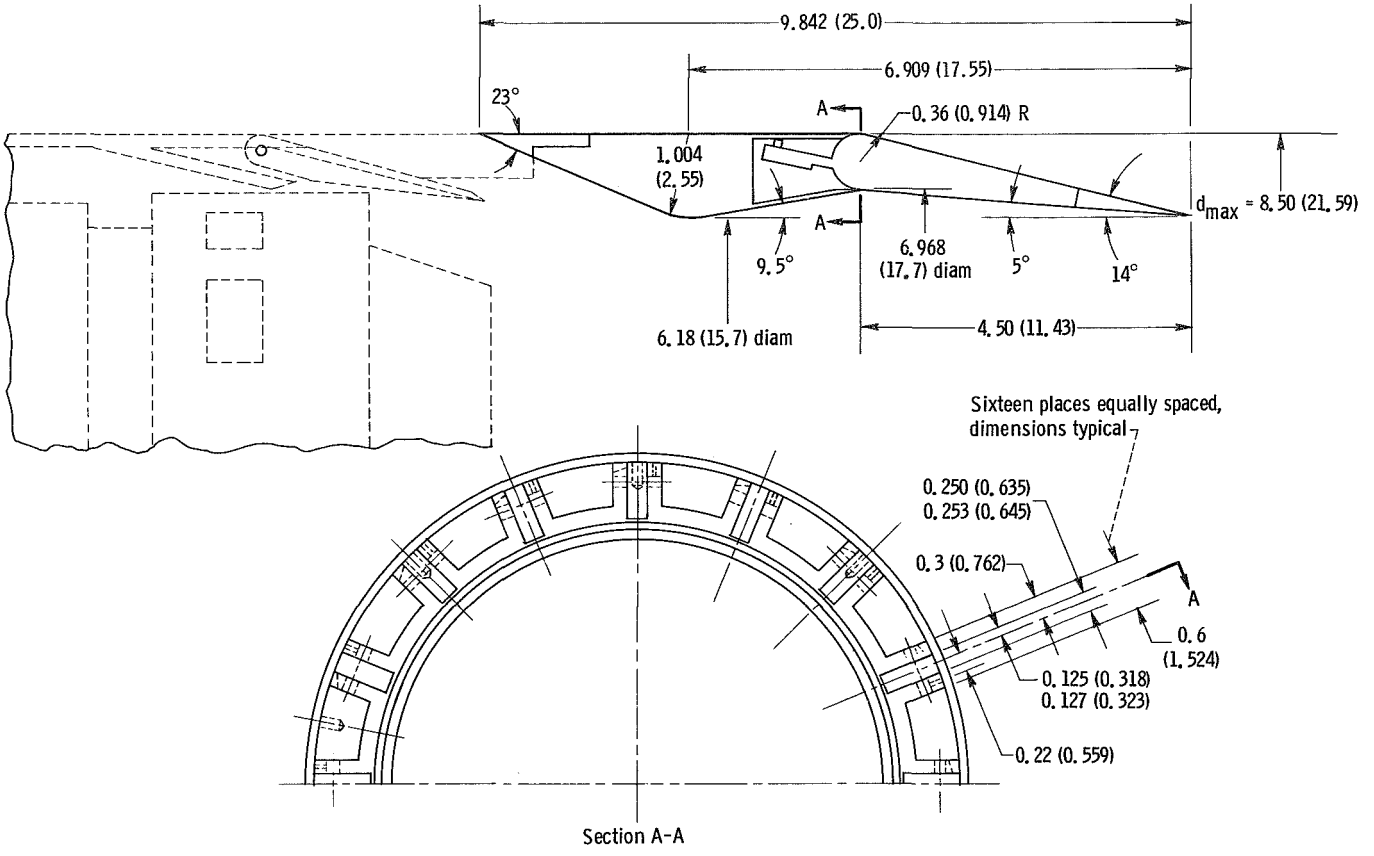

Figure 6. - Details of single-hinge trailing-edge flap. (Dimensions are in inches (cm).)

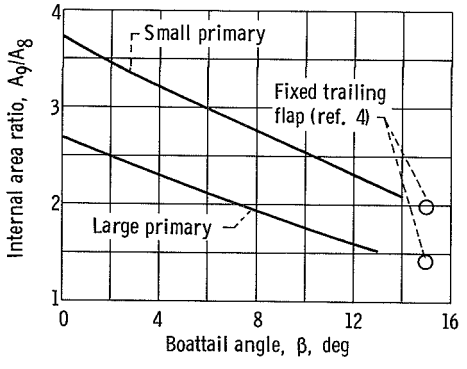

Figure 7. - Variation of internal expansion ratio with boattail angle.

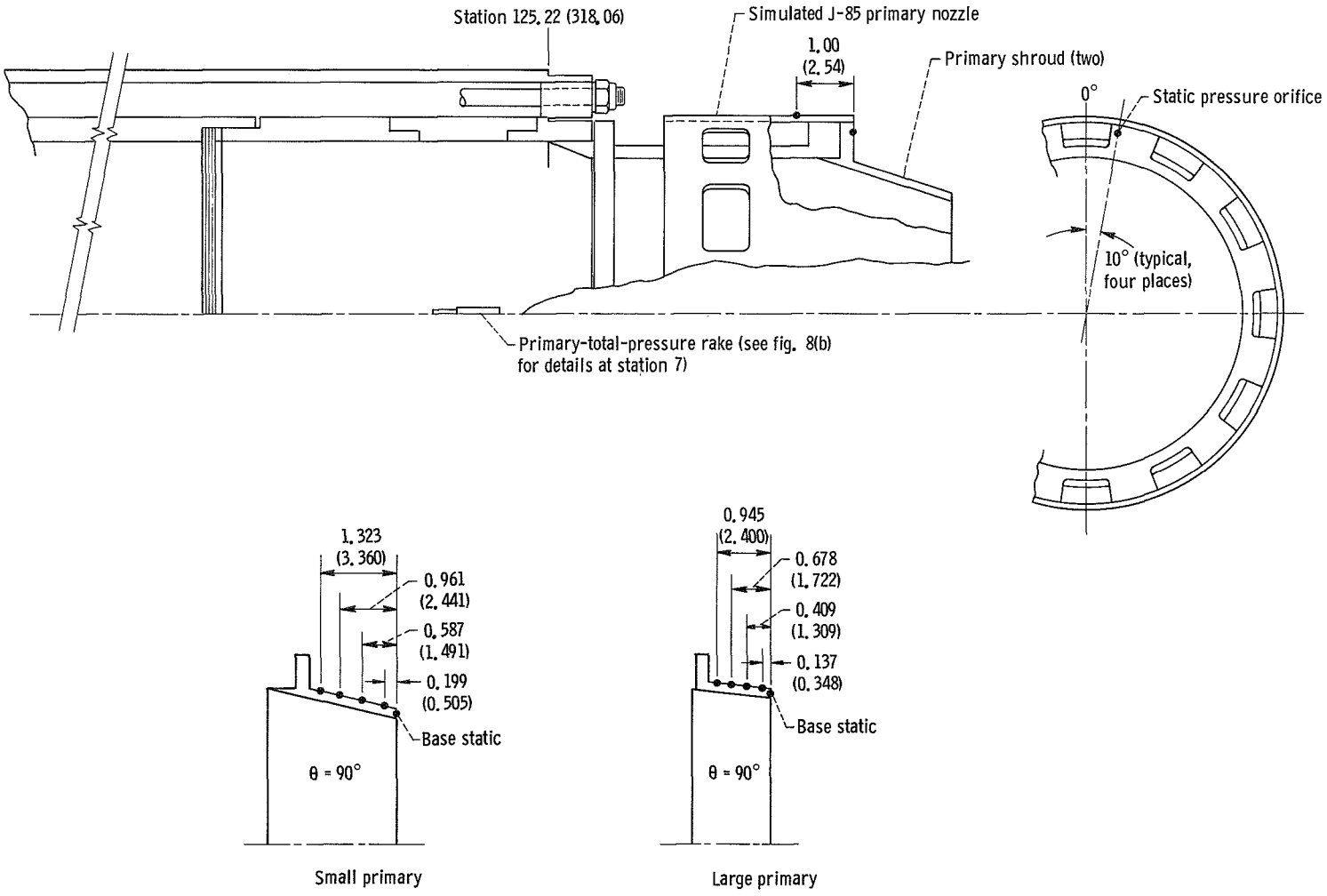

(a) Secondary air and primary nozzle

Figure 8. - Nozzle instrumentation details. (Dimensions are in inches (cm).)

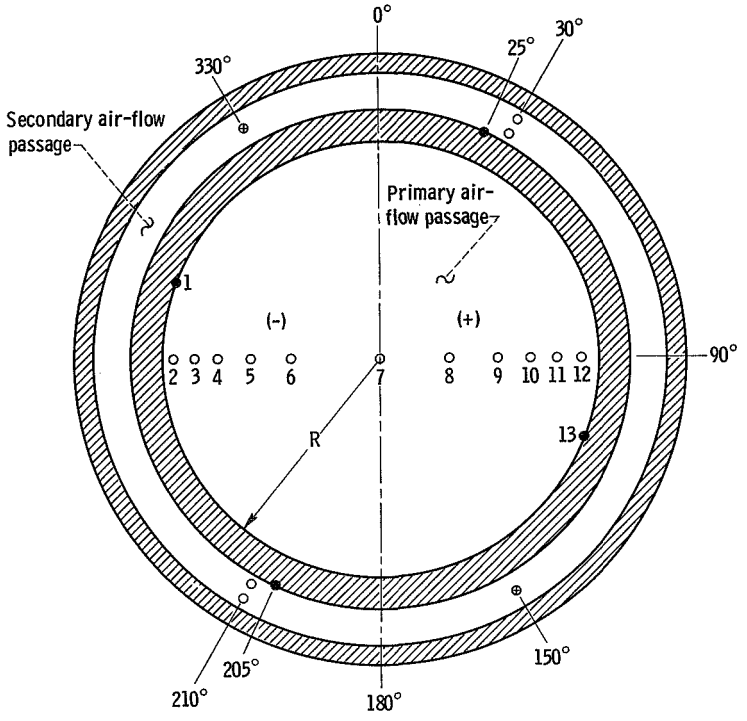

Primary flow orifice number	Normalized distance from centerline, r/R^a
1	-1.000
2	-.950
3	-.855
4	-.750
5	-.600
6	-.418
7	0
8	.300
9	.519
10	.670
11	.790
12	.900
13	1.000

[a] R = 3.006 in. (7.635 cm); r is radius from centerline to the local orifice.

● Static-pressure orifice
○ Total-pressure orifice
⊕ Thermocouple

(b) Station 7.

Figure 8. - Continued.

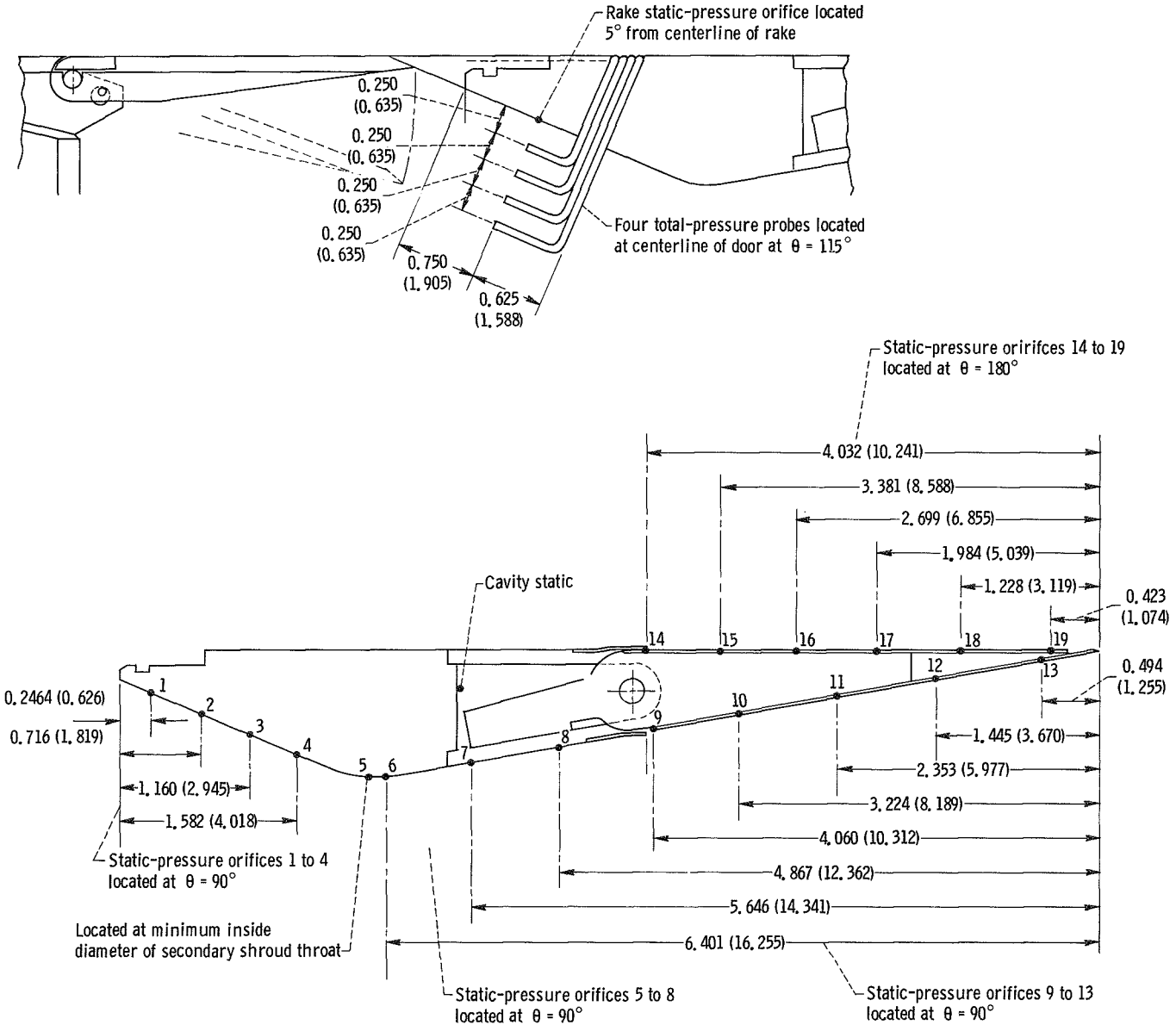

(c) Secondary shroud instrumentation.

Figure 8. - Continued.

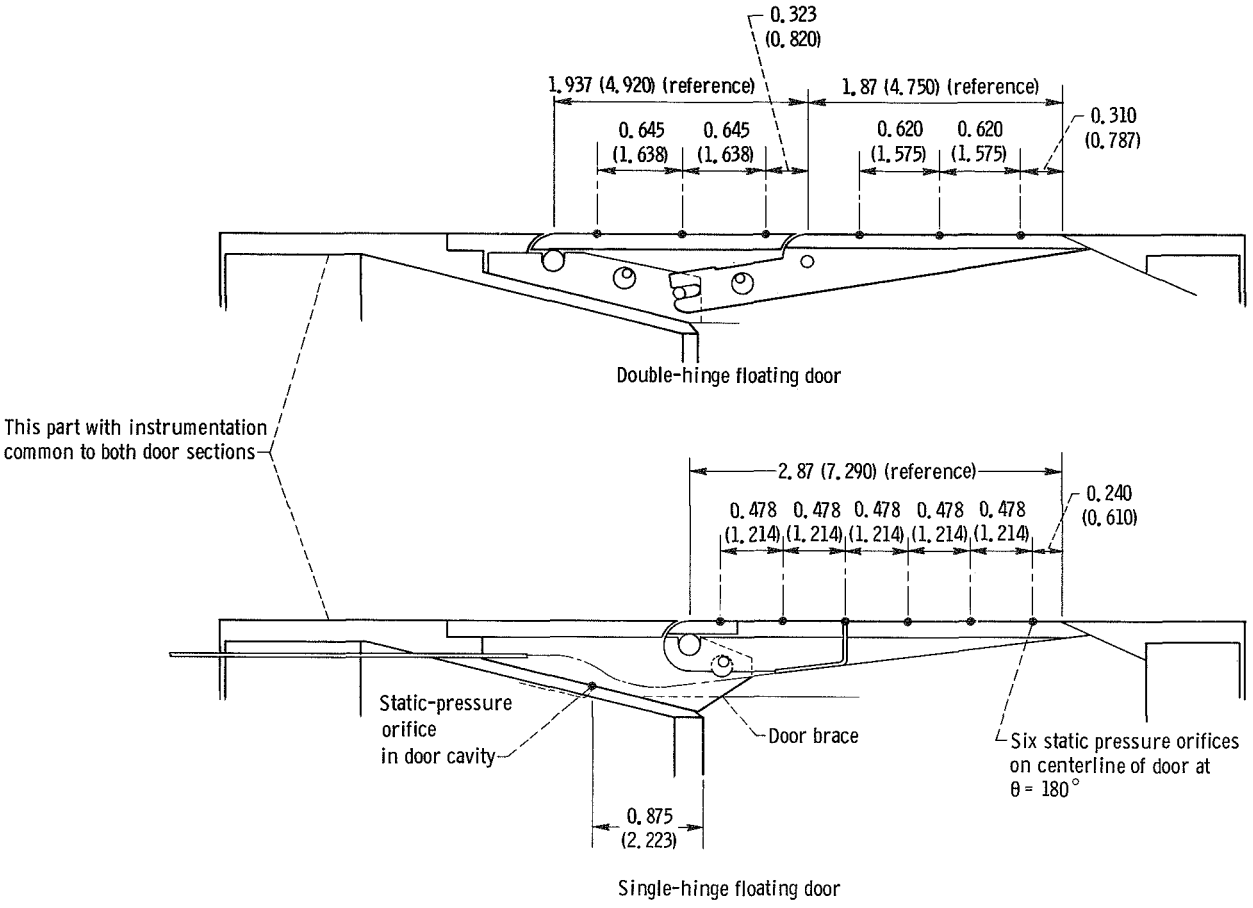

(d) Auxiliary inlet instrumentation.

Figure 8. - Concluded.

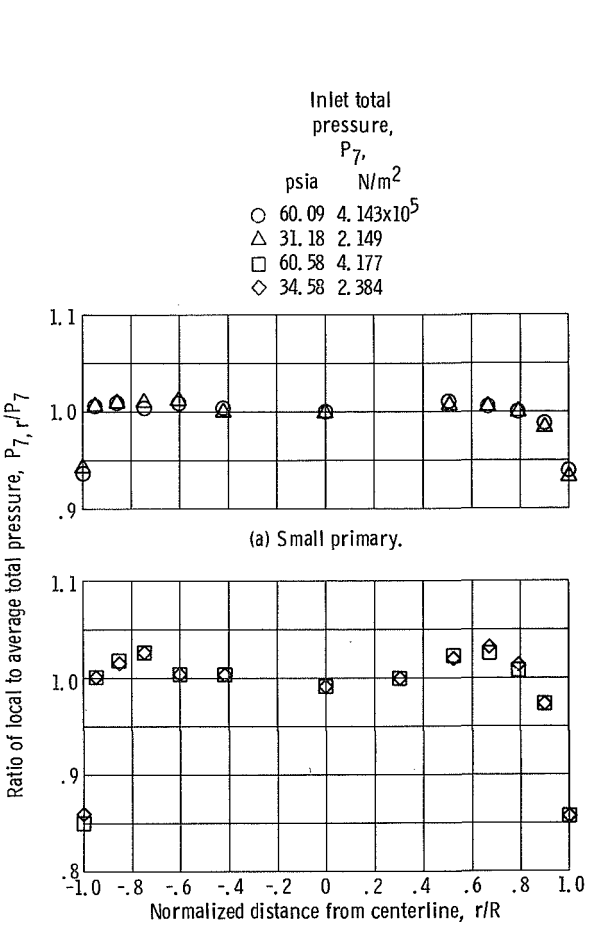

(a) Small primary.

(b) Large primary.

Figure 9. - Primary air total-pressure profile at station 7.

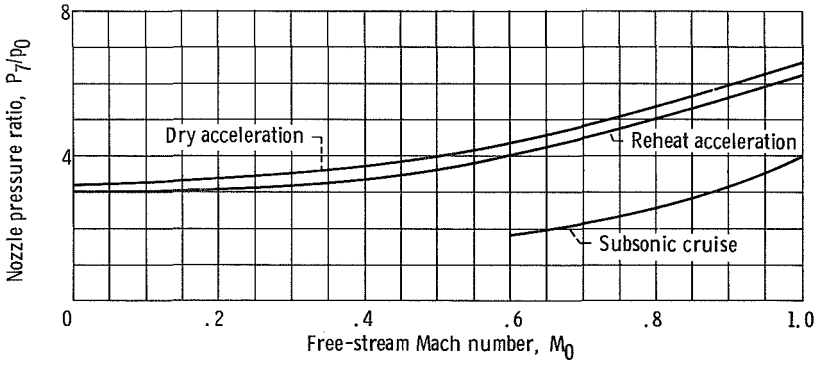

Figure 10. - Schedule of turbojet nozzle pressure ratio with free-stream Mach number.

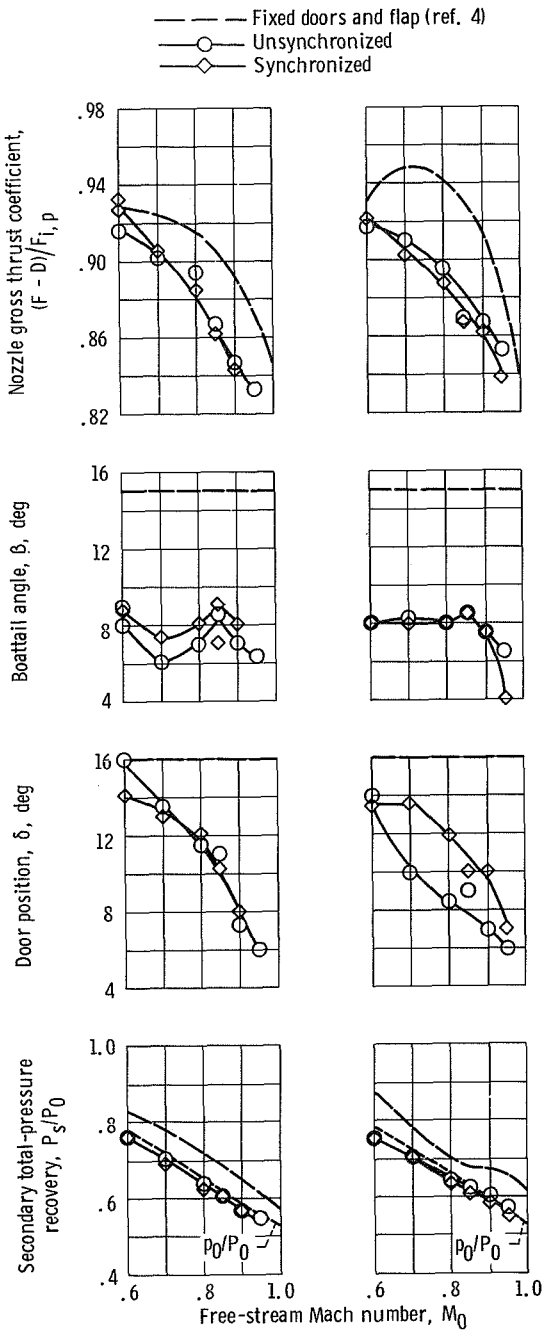

(a) Single-hinge doors.

(b) Double-hinge doors (δ_2/δ_1 = 2/1).

Figure 11. - Comparison at subsonic cruise of performance with aerodynamically positioned doors and flaps to peak performance obtained with fixed components. Small primary; corrected-secondary-weight-flow ratio, $\omega\sqrt{\theta} = 0.04$.

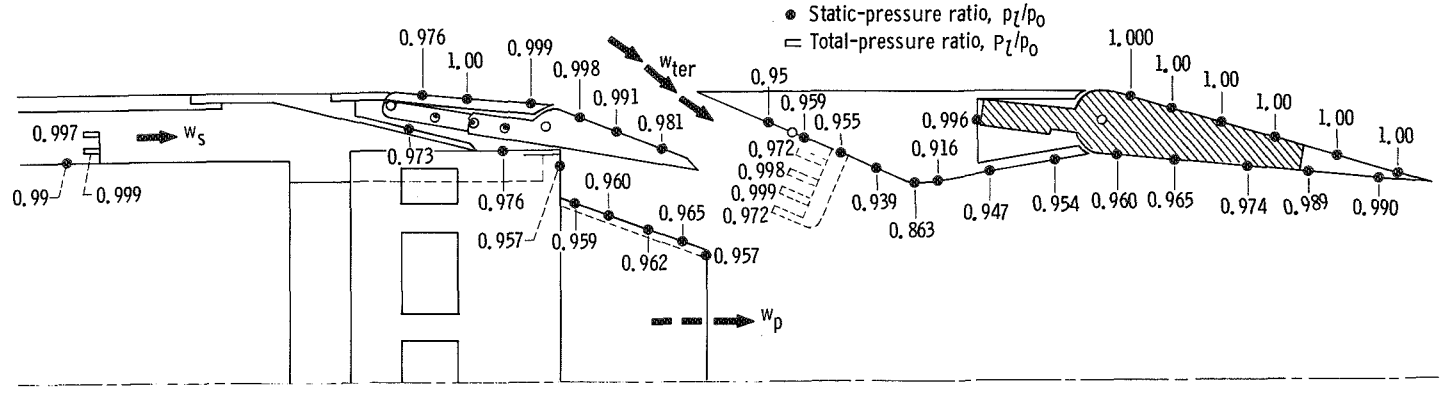

(a) Free-stream Mach number, $M_0 = 0$; nozzle pressure ratio, $P_7/p_0 = 3.24$; corrected-secondary-weight-flow ratio, $\omega\sqrt{\tau} = 0.039$; boattail angle, $\beta = 14°$; door angle, $\delta = 8°$-$16°$; nozzle gross thrust coefficient, $(F - D)/F_{i,p} = 1.00$.

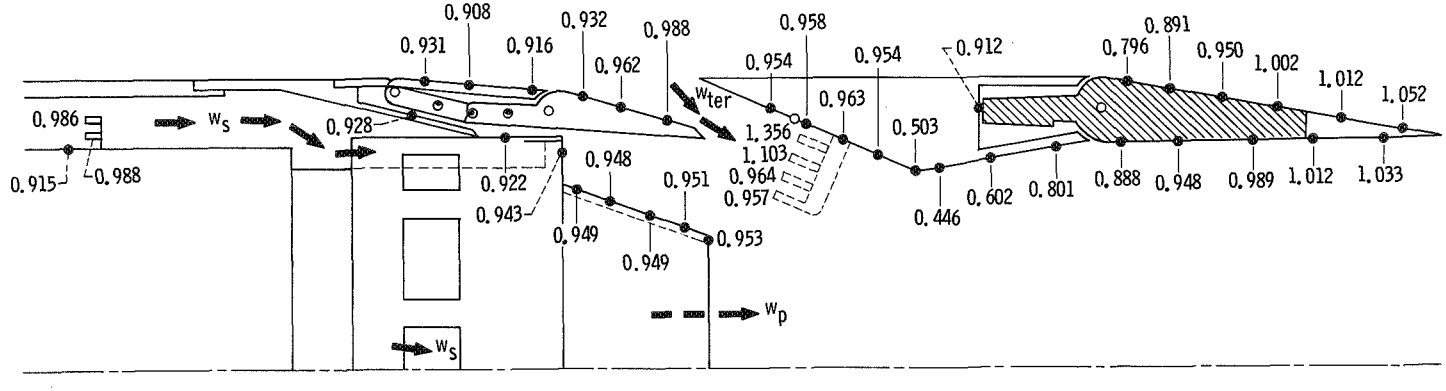

(b) Free-stream Mach number, $M_0 = 0.90$; nozzle pressure ratio, $P_7/p_0 = 3.15$; corrected-secondary-weight-flow ratio, $\omega\sqrt{\tau} = 0.044$; boattail angle, $\beta = 8°$; door angle, $\delta = 5°$-$10°$; nozzle gross thrust coefficient, $(F - D)/F_{i,p} = 0.86$.

Figure 12. - Effect of external flow on auxiliary inlet ejector nozzle pressure distribution. Double-hinge synchronized doors (2/1).

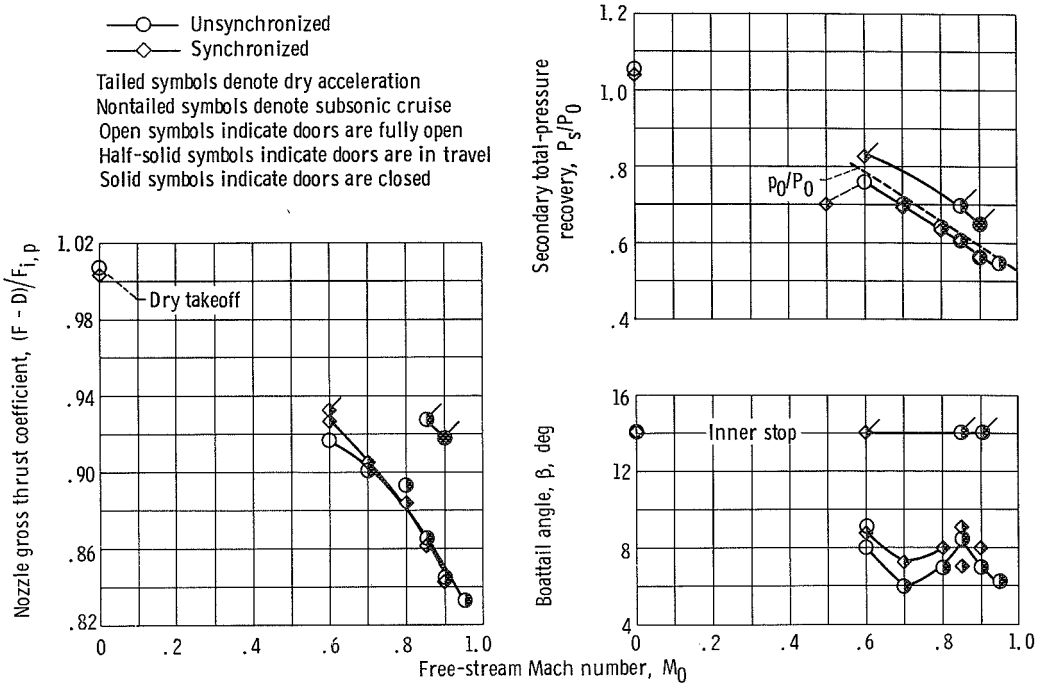

Figure 13. - Performance of single-hinge inlet door configurations. Small primary; corrected-secondary-weight-flow ratio $\omega\sqrt{\tau} = 0.042$.

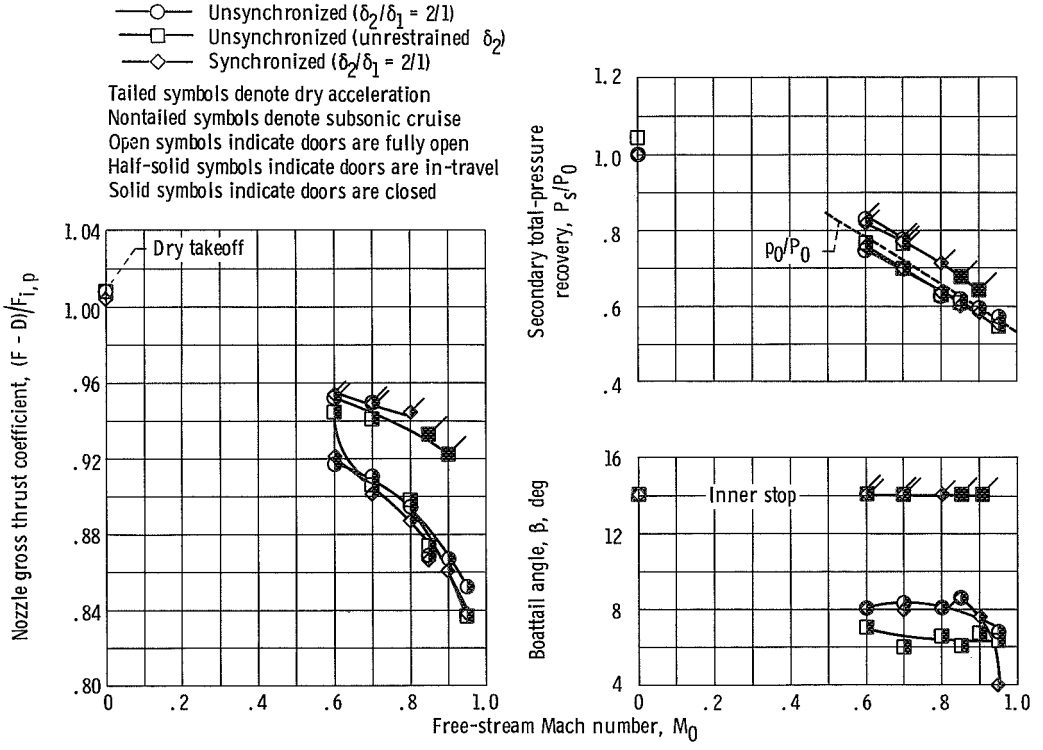

Figure 14. - Performance of double-hinge inlet door configuration. Small primary; corrected-secondary-weight-flow ratio, $\omega\sqrt{\tau} = 0.042$.

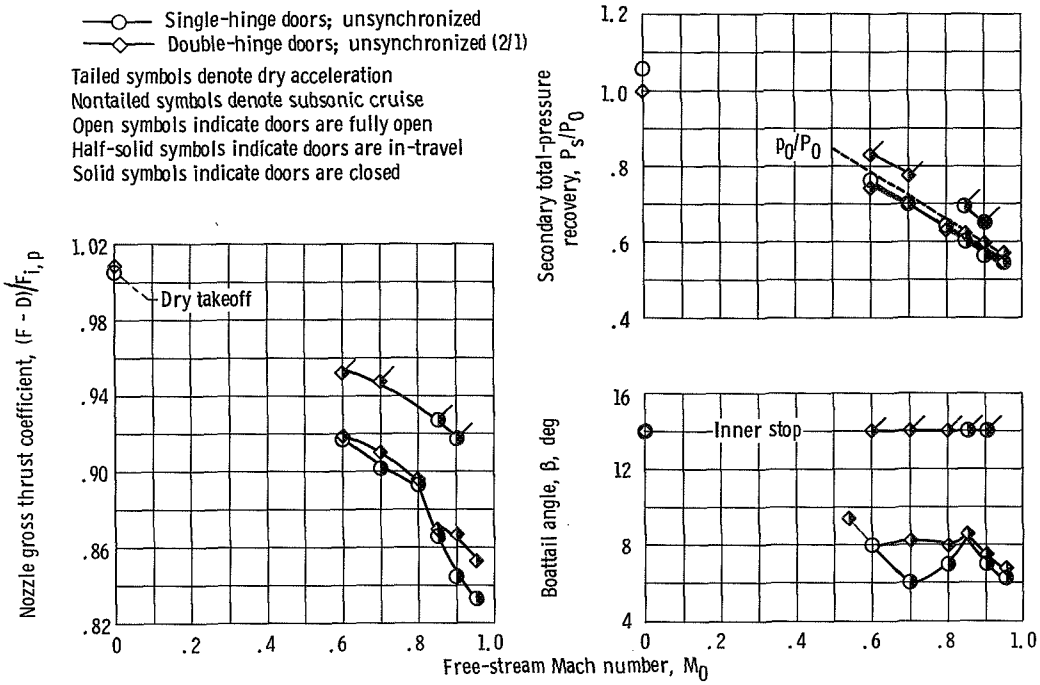

Figure 15. - Comparison of best performance single- and double-hinge door configurations. Small primary; corrected-secondary-weight-flow ratio, $\omega\sqrt{\theta} = 0.042$.

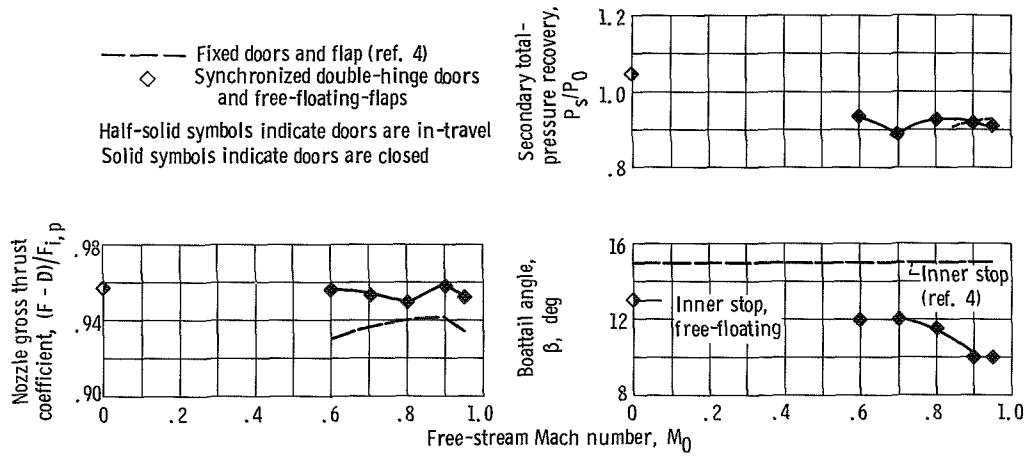

Figure 16. - Performance characteristics of inlet door configuration during reheat operation. Large primary; corrected-secondary-weight-flow ratio, $\omega\sqrt{\theta} = 0.04$.

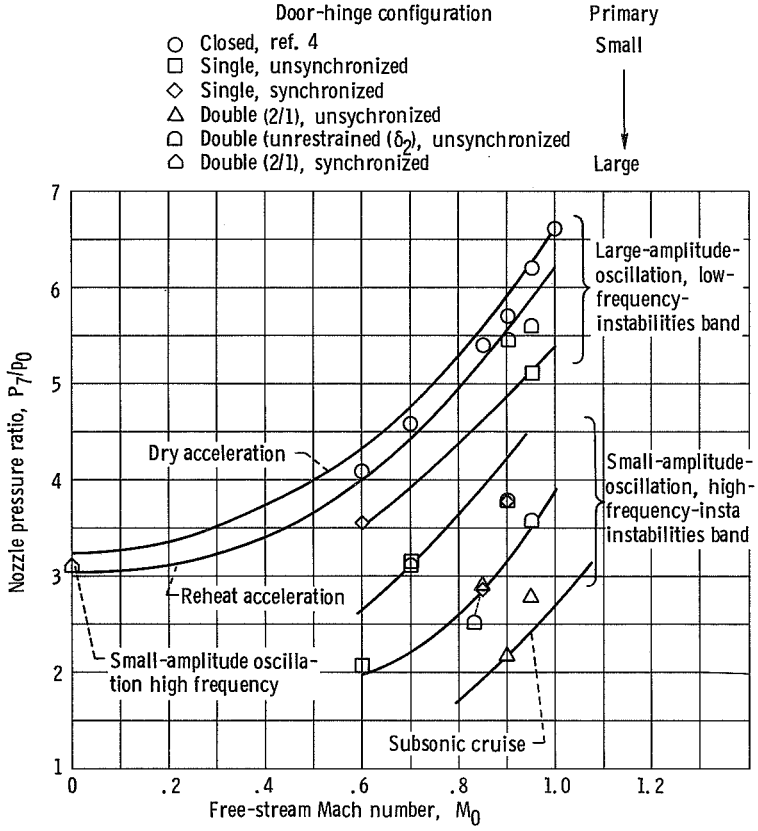

Figure 17. - Nozzle trailing-edge-flap instabilities over the flight trajectories with a nominal corrected secondary weight flow of 4 percent.

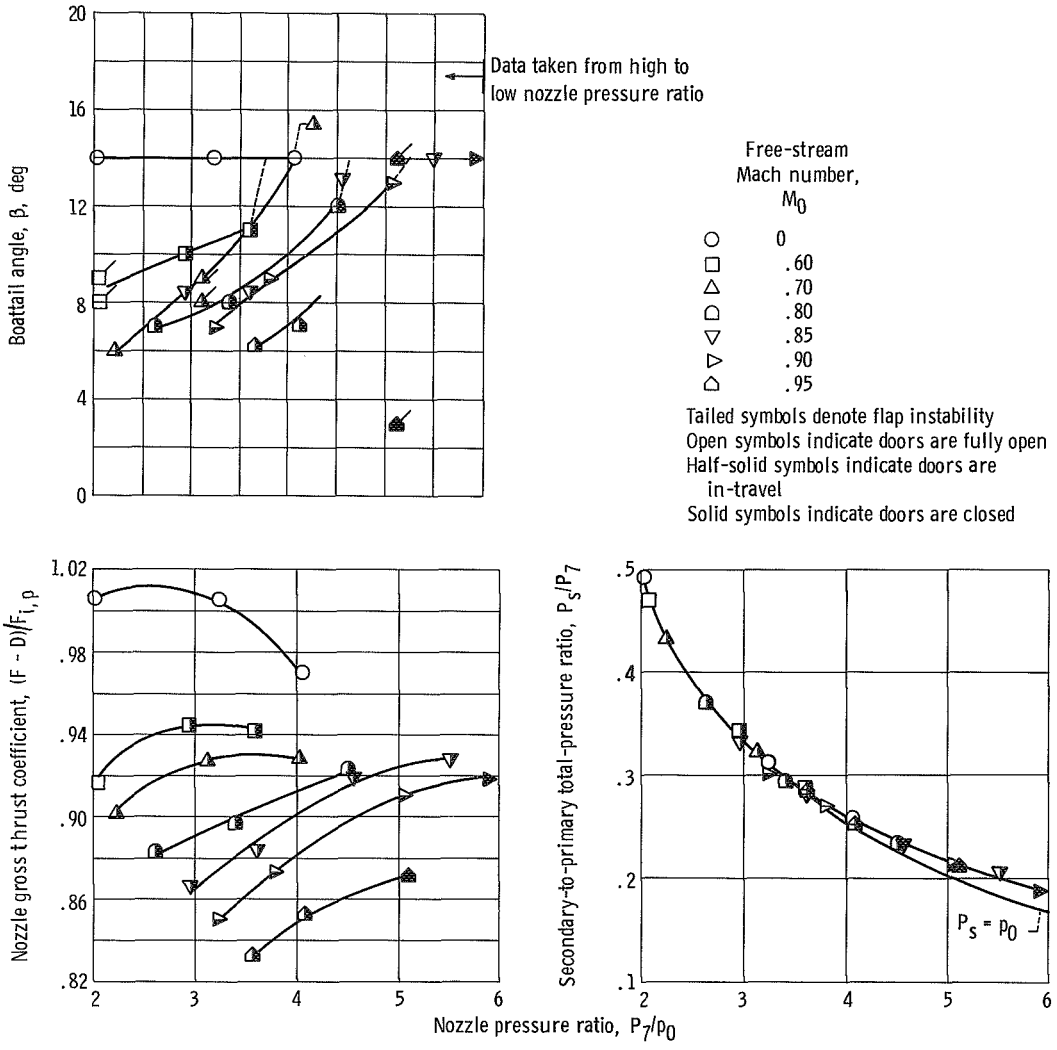

(a) Single-hinge doors, unsynchronized.

Figure 18. - Effect of nozzle pressure ratio on single-hinge-door-configuration performance. Small primary; corrected-secondary-weight-flow ratio, $\omega\sqrt{\theta} = 0.04$.

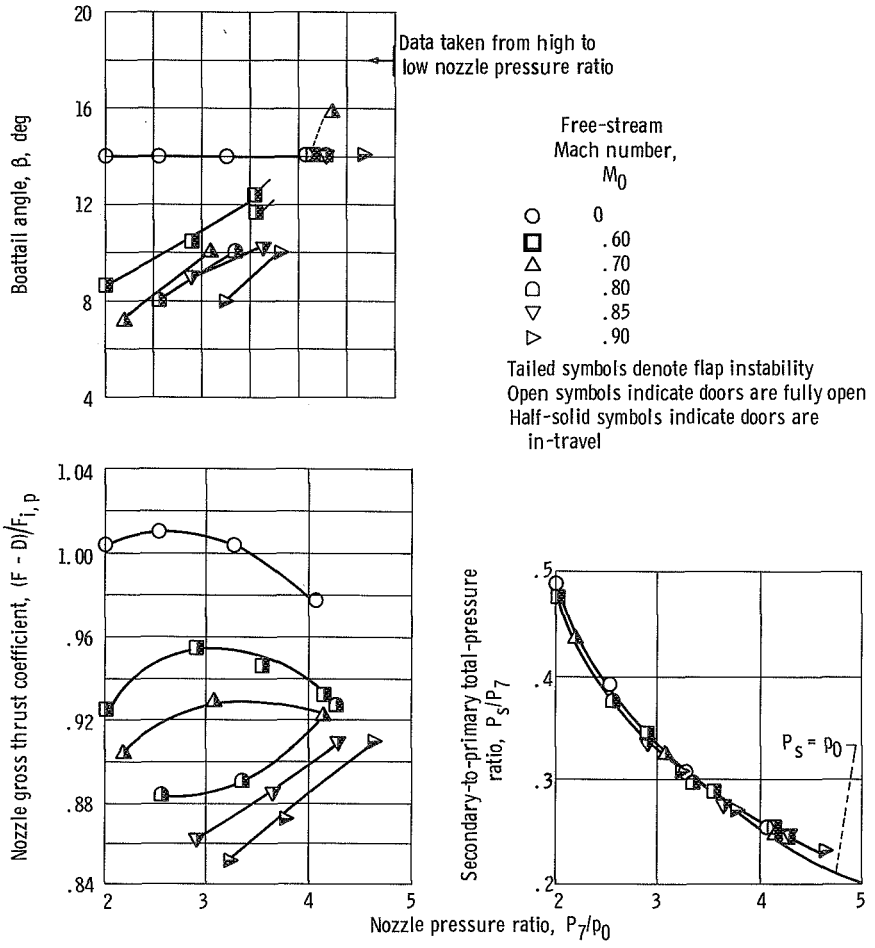

(b) Single-hinge doors, synchronized.

Figure 18. - Concluded.

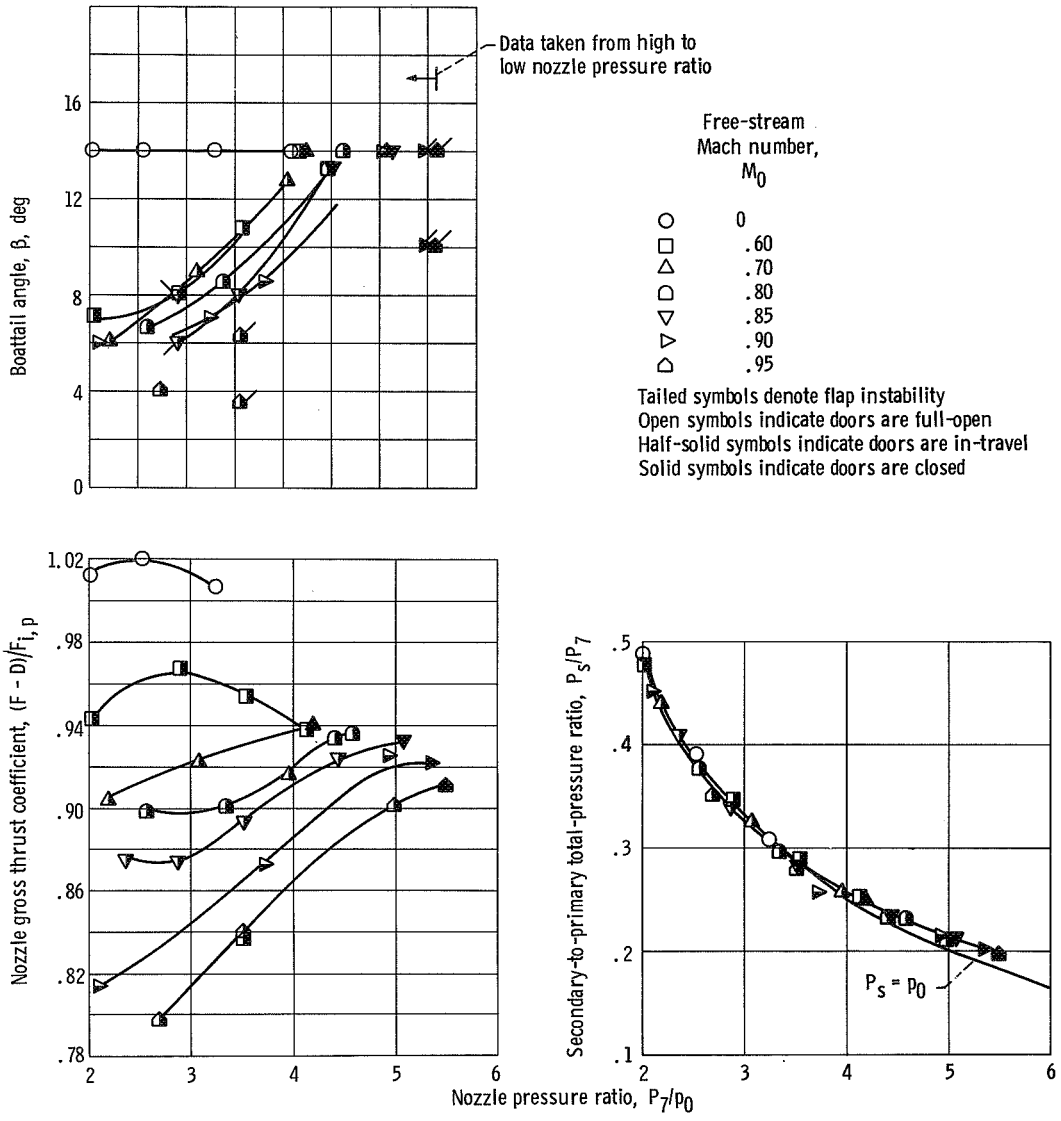

(a) Double-hinge doors, unsynchronized, unrestrained δ_2; small primary.

Figure 19. - Effect of nozzle pressure ratio on the double-hinge-door-configuration performance. Corrected-secondary-weight-flow ratio, $\omega\sqrt{\tau} = 0.04$.

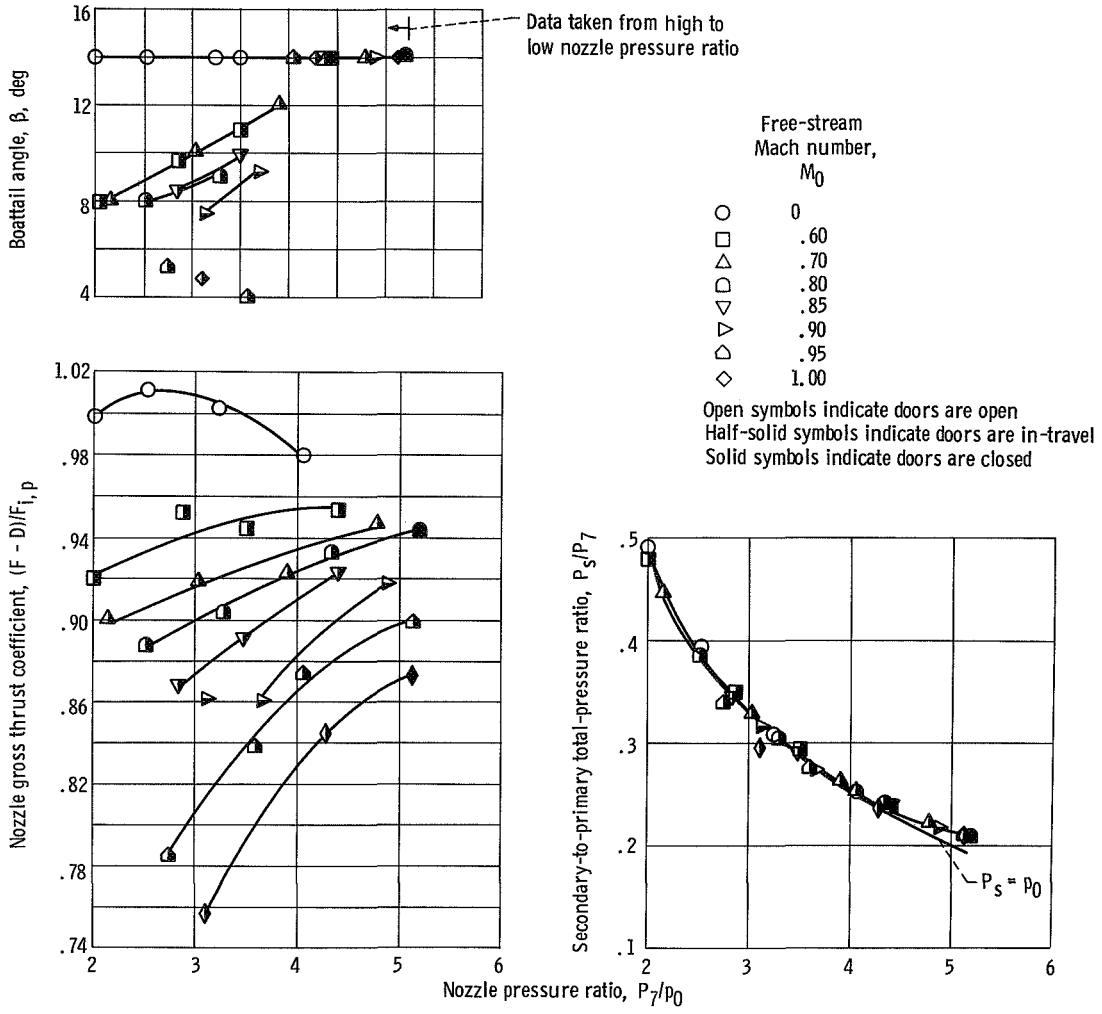

(b) Double-hinge doors, synchronized (2/1); small primary.

Figure 19. - Continued.

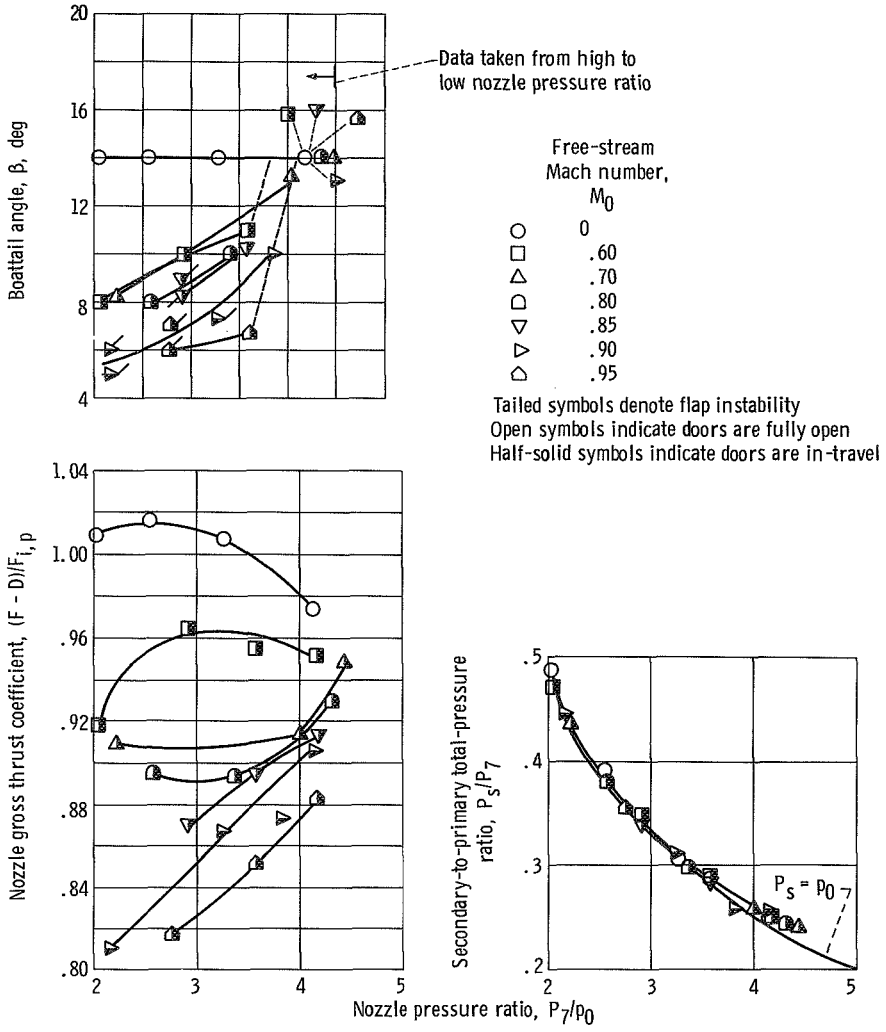

(c) Double-hinge doors, unsynchronized (2/1); small primary.

Figure 19. - Continued.

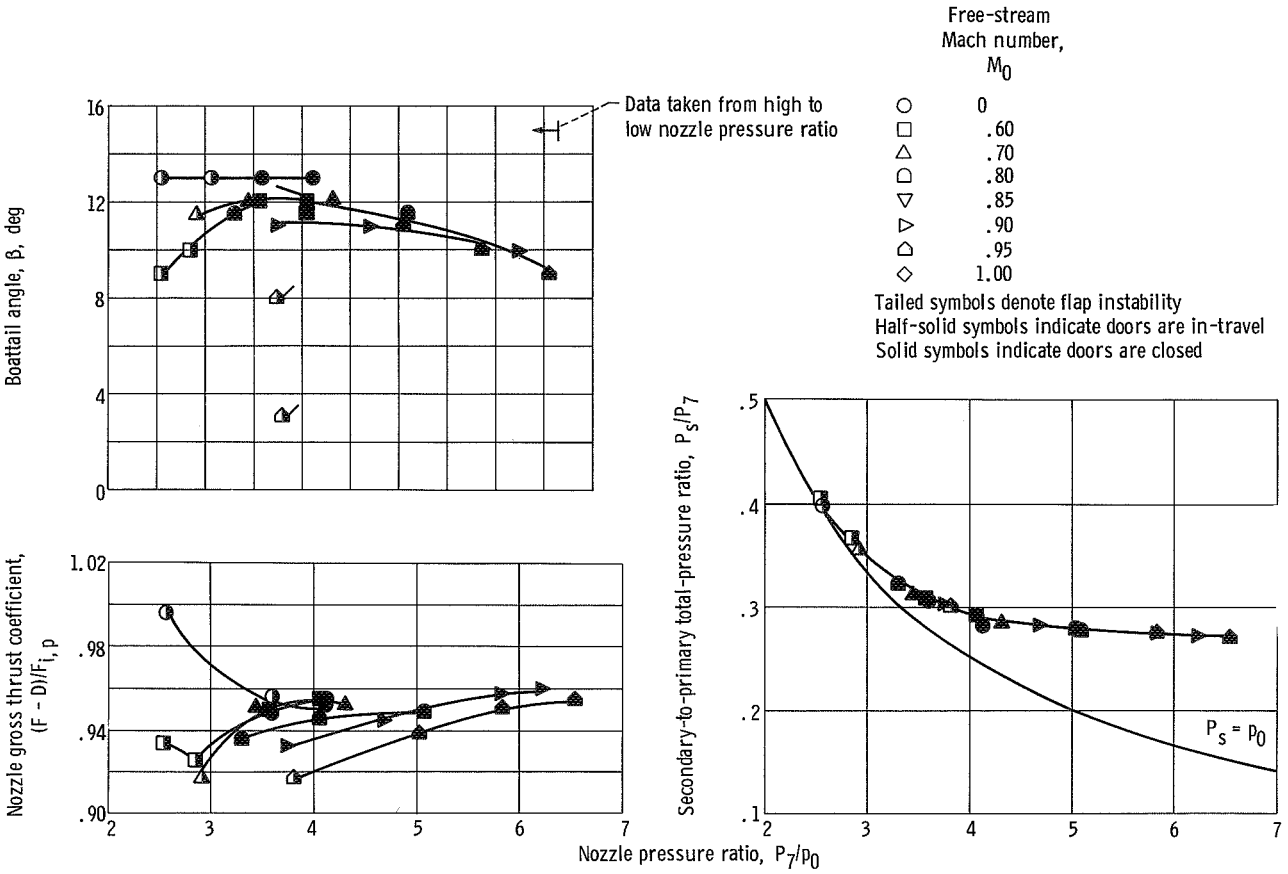

(d) Double-hinge doors, synchronized (2/1); large primary.

Figure 19. - Concluded.

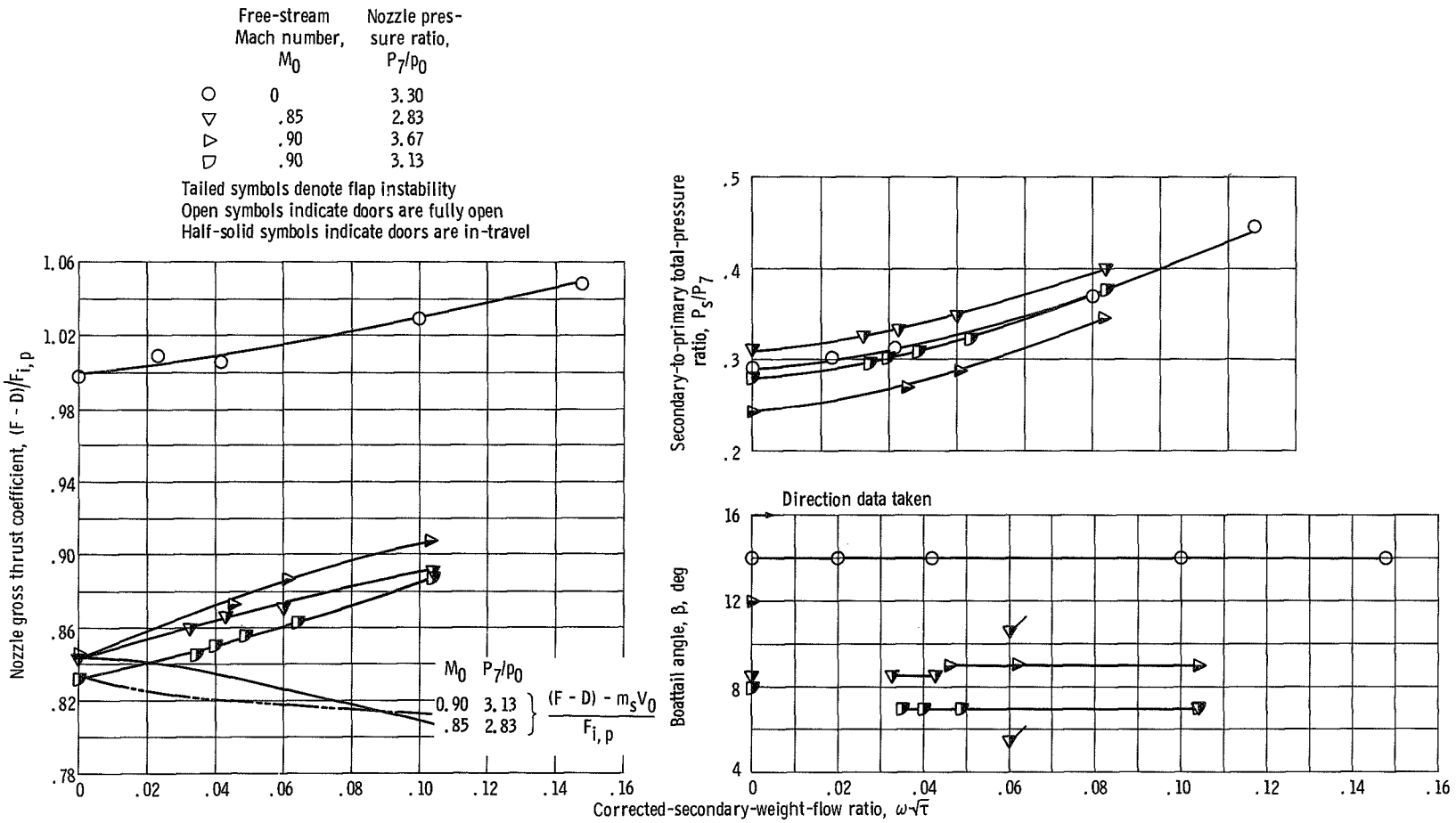

(a) Single-hinge doors, unsynchronized.

Figure 20. - Effect of corrected-secondary-weight-flow ratio on single-hinge-door-configuration nozzle performance. Small primary.

	Free-stream Mach number, M_0	Nozzle pressure ratio, P_7/p_0
○	0	3.30
▽	.85	2.83
▷	.90	3.67
▱	.90	3.13

Tailed symbols denote flap instability
Open symbols indicate doors are fully open
Half-solid symbols indicate doors are in-travel

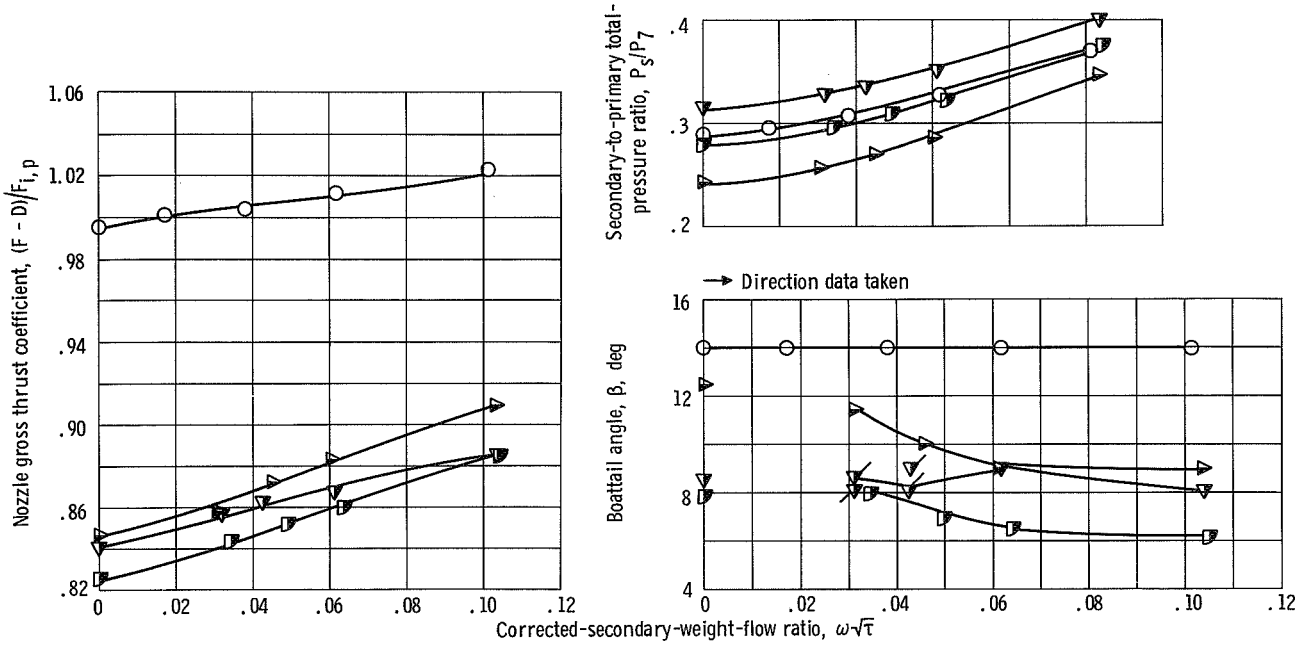

(b) Single-hinge doors, synchronized.

Figure 20. - Concluded.

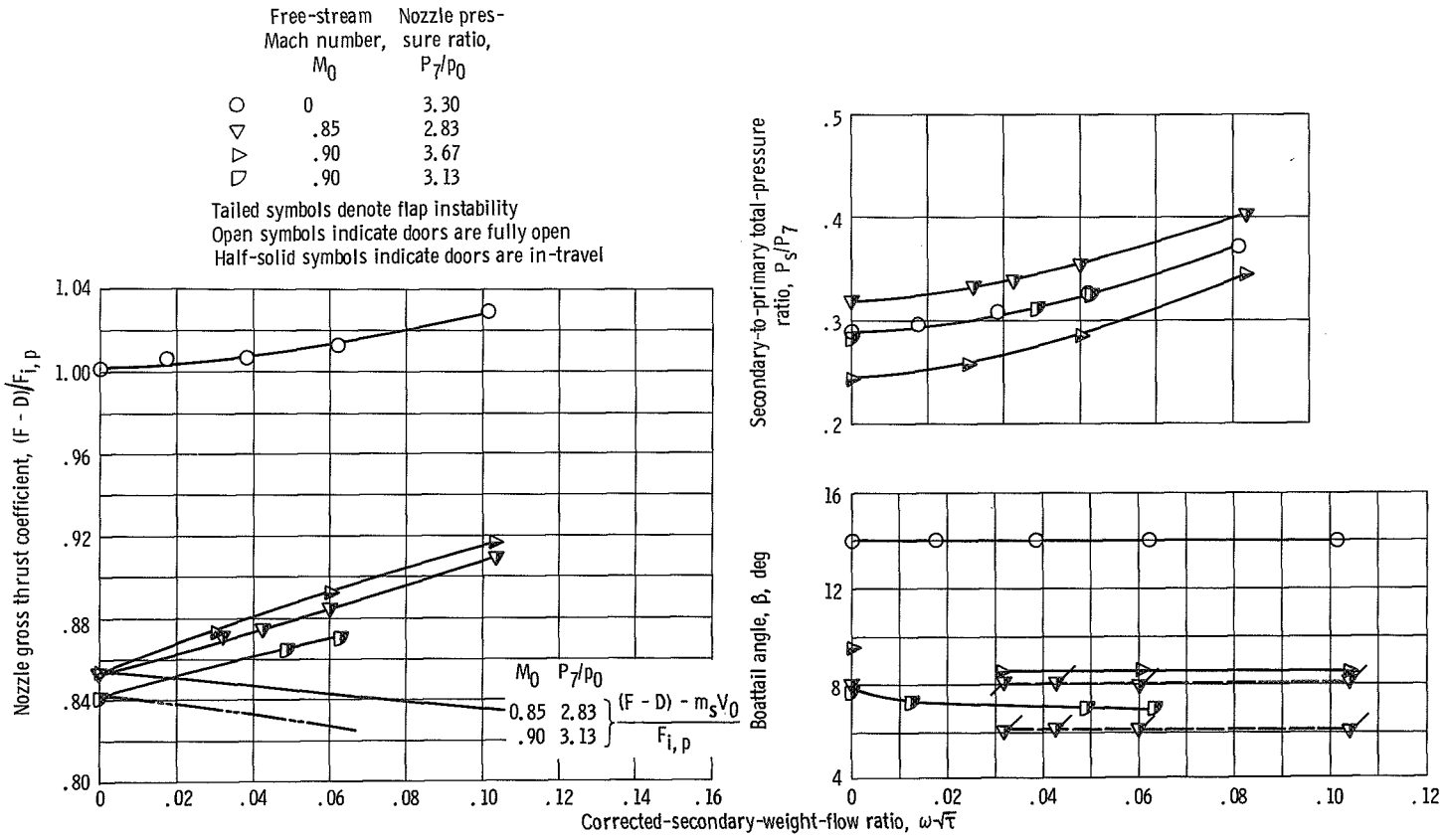

(a) Double-hinge doors, unsynchronized, unrestrained δ_2; small primary.

Figure 21. - Effect of corrected-secondary-weight-flow ratio on double-hinge-door-configuration nozzle performance.

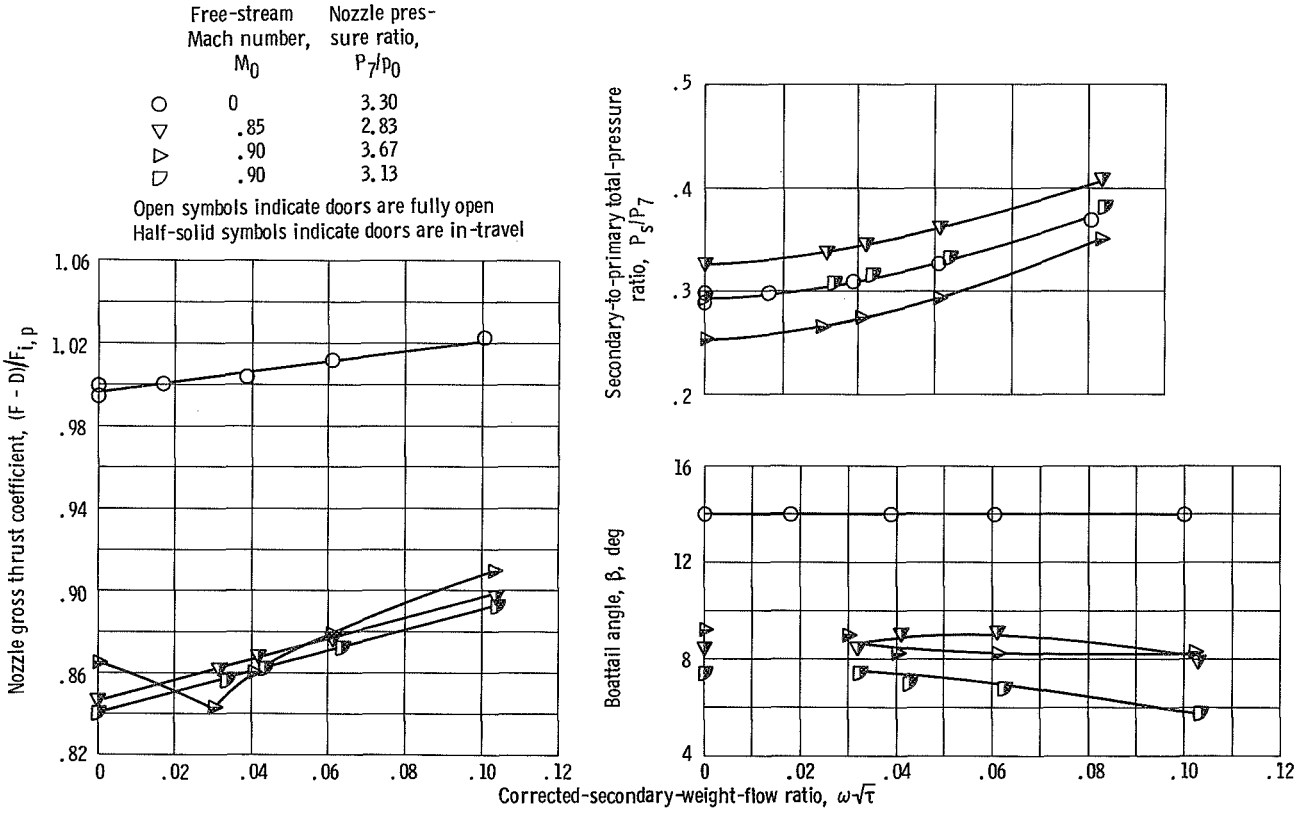

(b) Double-hinge doors, synchronized; small primary.

Figure 21. - Continued.

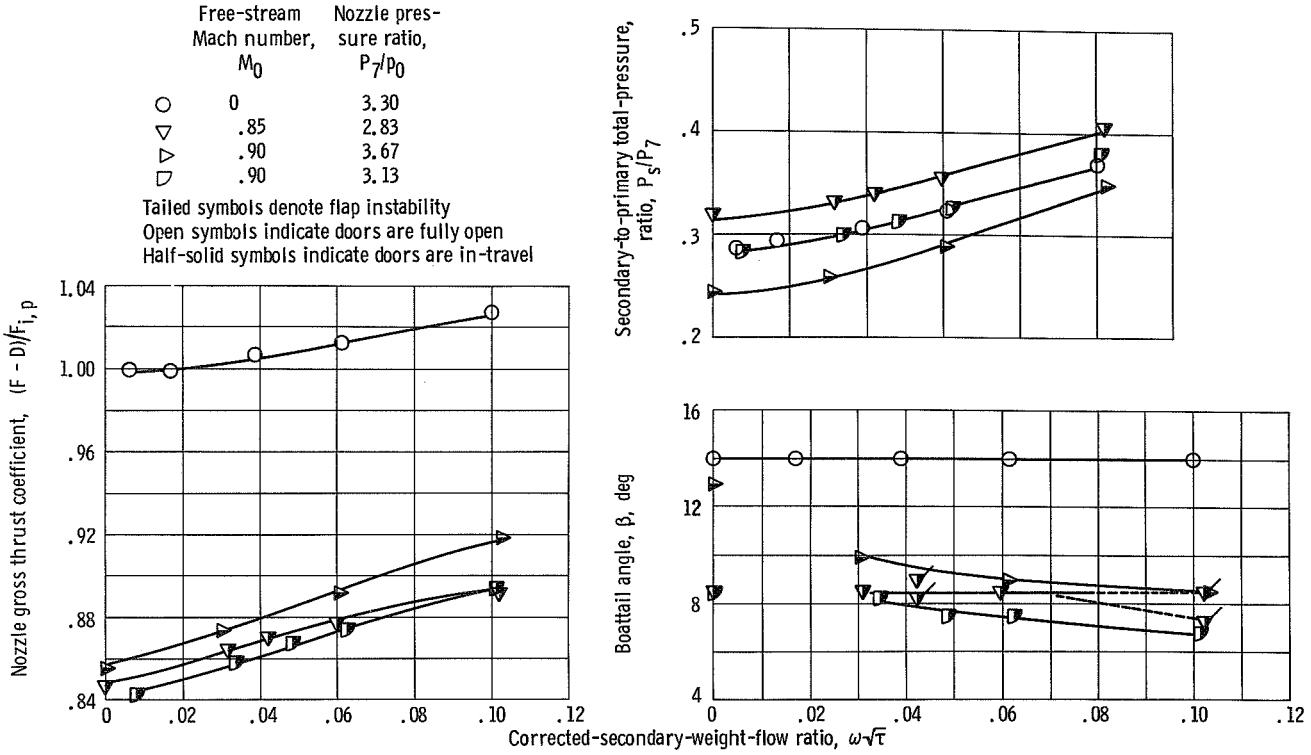

(c) Double-hinge doors, unsynchronized (2/1); small primary.

Figure 21. - Continued.

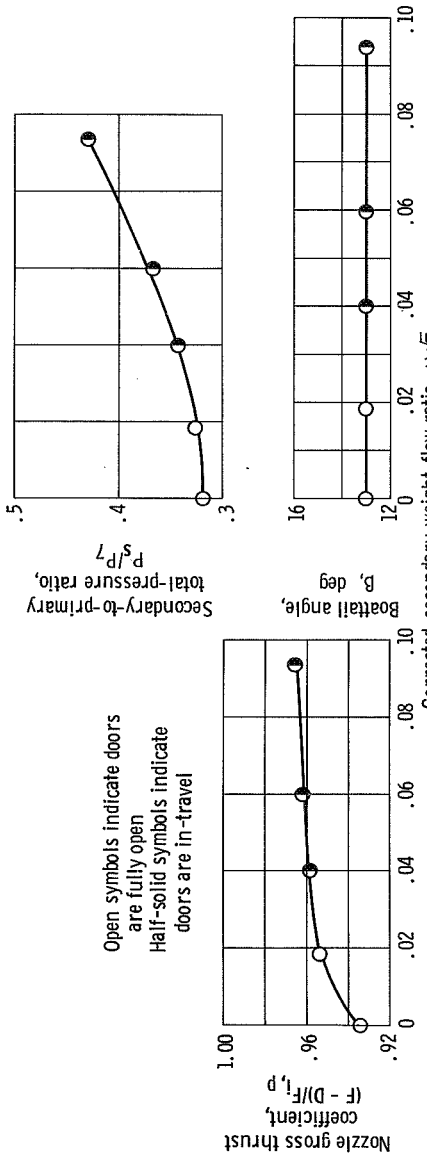

(d) Double-hinge doors, unsynchronized; large primary; free-stream Mach number, $M_0 = 0$; nozzle pressure ratio, $P_7/p_0 = 3.30$.

Figure 21. - Concluded.

1. Report No.	2. Government Accession No.	3. Recipient's Catalog No.
NASA TM X-2173		

4. Title and Subtitle	5. Report Date
PERFORMANCE OF AN AUXILIARY INLET EJECTOR NOZZLE WITH FLOATING INLET DOORS AND FLOATING SINGLE-HINGE TRAILING-EDGE FLAPS	February 1971
	6. Performing Organization Code
7. Author(s)	8. Performing Organization Report No.
Albert L. Johns	E-5883
	10. Work Unit No.
9. Performing Organization Name and Address	720-03
Lewis Research Center National Aeronautics and Space Administration Cleveland, Ohio 44135	11. Contract or Grant No.
	13. Type of Report and Period Covered
12. Sponsoring Agency Name and Address	Technical Memorandum
National Aeronautics and Space Administration Washington, D. C. 20546	14. Sponsoring Agency Code

15. Supplementary Notes

16. Abstract

A nozzle designed for a supersonic-cruise aircraft was tested at off-design Mach numbers from 0 to 1.0. Two primary throat areas were tested: one to simulate both dry acceleration and subsonic cruise, and the other to simulate reheat acceleration. The auxiliary inlet doors included single- and double-hinge types which were free-floating either with or without synchronization. Results from this cold-flow model are compared with a similar nozzle which was optimized using fixed inlet doors and flaps. The inlet doors and trailing-edge flaps did not float to the maximum thrust condition at subsonic-cruise Mach numbers. In addition, the single-hinge flaps were unstable at many of the assumed flight conditions.

17. Key Words (Suggested by Author(s))	18. Distribution Statement
Propulsion Ejector nozzle	Unclassified - unlimited

19. Security Classif. (of this report)	20. Security Classif. (of this page)	21. No. of Pages	22. Price*
Unclassified	Unclassified	45	$3.00

*For sale by the National Technical Information Service, Springfield, Virginia 22151

NATIONAL AERONAUTICS AND SPACE ADMINISTRATION
WASHINGTON, D.C. 20546

OFFICIAL BUSINESS

FIRST CLASS MAIL

POSTAGE AND FEES PAID
NATIONAL AERONAUTICS A
SPACE ADMINISTRATION

POSTMASTER: If Undeliverable (Section 15
Postal Manual) Do Not Ret

"The aeronautical and space activities of the United States shall be conducted so as to contribute . . . to the expansion of human knowledge of phenomena in the atmosphere and space. The Administration shall provide for the widest practicable and appropriate dissemination of information concerning its activities and the results thereof."

—NATIONAL AERONAUTICS AND SPACE ACT OF 1958

NASA SCIENTIFIC AND TECHNICAL PUBLICATIONS

TECHNICAL REPORTS: Scientific and technical information considered important, complete, and a lasting contribution to existing knowledge.

TECHNICAL NOTES: Information less broad in scope but nevertheless of importance as a contribution to existing knowledge.

TECHNICAL MEMORANDUMS: Information receiving limited distribution because of preliminary data, security classification, or other reasons.

CONTRACTOR REPORTS: Scientific and technical information generated under a NASA contract or grant and considered an important contribution to existing knowledge.

TECHNICAL TRANSLATIONS: Information published in a foreign language considered to merit NASA distribution in English.

SPECIAL PUBLICATIONS: Information derived from or of value to NASA activities. Publications include conference proceedings, monographs, data compilations, handbooks, sourcebooks, and special bibliographies.

TECHNOLOGY UTILIZATION PUBLICATIONS: Information on technology used by NASA that may be of particular interest in commercial and other non-aerospace applications. Publications include Tech Briefs, Technology Utilization Reports and Technology Surveys.

Details on the availability of these publications may be obtained from:

SCIENTIFIC AND TECHNICAL INFORMATION OFFICE

NATIONAL AERONAUTICS AND SPACE ADMINISTRATION

Washington, D.C. 20546